Article

The Mechanism of Phagocytosis: Two Stages of Engulfment

David M. Richards[1,2,*] and Robert G. Endres[1,2]
[1]Department of Life Sciences and [2]Centre for Integrative Systems Biology and Bioinformatics, Imperial College, London, United Kingdom

ABSTRACT Despite being of vital importance to the immune system, the mechanism by which cells engulf relatively large solid particles during phagocytosis is still poorly understood. From movies of neutrophil phagocytosis of polystyrene beads, we measure the fractional engulfment as a function of time and demonstrate that phagocytosis occurs in two distinct stages. During the first stage, engulfment is relatively slow and progressively slows down as phagocytosis proceeds. However, at approximately half-engulfment, the rate of engulfment increases dramatically, with complete engulfment attained soon afterwards. By studying simple mathematical models of phagocytosis, we suggest that the first stage is due to a passive mechanism, determined by receptor diffusion and capture, whereas the second stage is more actively controlled, perhaps with receptors being driven toward the site of engulfment. We then consider a more advanced model that includes signaling and captures both stages of engulfment. This model predicts that there is an optimum ligand density for quick engulfment. Further, we show how this model explains why nonspherical particles engulf quickest when presented tip-first. Our findings suggest that active regulation may be a later evolutionary innovation, allowing fast and robust engulfment even for large particles.

INTRODUCTION

Cells have evolved a whole host of mechanisms for ingesting particles and fluids. These vary from receptor-mediated endocytosis (absorption of small particles into clathrin-coated vesicles), to pinocytosis (the uptake of soluble material), to phagocytosis. Phagocytosis is the mechanism by which relatively large ($>0.5\ \mu$m) particles, such as bacteria, dead cells, or (as here) polystyrene beads, are internalized (1–3). During phagocytosis in immune cells such as neutrophils and macrophages, receptors in the cell membrane first recognize antibodies on the target, which causes membrane protrusions called pseudopodia to surround the target in a zipperlike mechanism (see Fig. 1) (4,5). This is followed by fusion with lysosomes, acidification of the phagosome, and degradation of the target.

The most widely-studied example of phagocytosis involves Fcγ receptors, which recognize particles coated with immunoglobulin G (IgG) (6,7). Fcγ receptors are expressed in white blood cells in four different classes, distinguished by their antibody affinity (8). Upon binding to the Fc region of IgG, receptors signal via Syk kinases, small GTPases (9), and hundreds of other molecules, leading to substantial reorganization of the actin cytoskeleton and its contraction by multiple myosin isoforms (10,11). The resulting complexity (12) has the potential to obscure the fundamental processes and principles that, as often is the case in biology, may well be quite simple. In particular, the connection between fundamental physical mechanisms and biological regulation remains to be explained. Focusing on only the most important components, such as the receptors, ligand density, and particle shape, may help elucidate the fundamental underlying mechanisms of engulfment.

Despite phagocytosis being discovered more than 100 years ago (13), there are relatively few theoretical models of cup formation and receptor dynamics. In Herant et al. (14,15), finite-element computations were used to argue that engulfment requires two crucial interactions: 1), repulsion at the cup edge between the membrane and newly-polymerized actin; and 2), a flattening force within the cup. Conversely, van Zon et al. (16) modeled the motion of receptors and F-actin in an attempt to explain the fact that phagocytosis normally either fully completes or stalls before half-engulfment. In Tollis et al. (17), zipper-like engulfment was modeled as an actin-driven ratchet mechanism, leading to robust engulfment. However, none of these models allow for different physical and biological mechanisms to operate at different stages of engulfment.

In addition to these phagocytosis models, there is an elegant approach to modeling the related problem of endocytosis (18). This model maps the motion of receptors within the membrane to the well-known Stefan problem; in fact, to the supercooled Stefan problem. The Stefan problem, introduced in the nineteenth century, applies to first-order phase transitions governed by the heat equation. The archetypal example is that of the melting of ice, where the boundary between water and ice continually moves as more ice melts. This is remarkably similar to the cup

Submitted May 14, 2014, and accepted for publication July 22, 2014.

*Correspondence: d.richards@imperial.ac.uk

Editor: Dennis Bray.

0006-3495/14/10/1542/12 $2.00

http://dx.doi.org/10.1016/j.bpj.2014.07.070

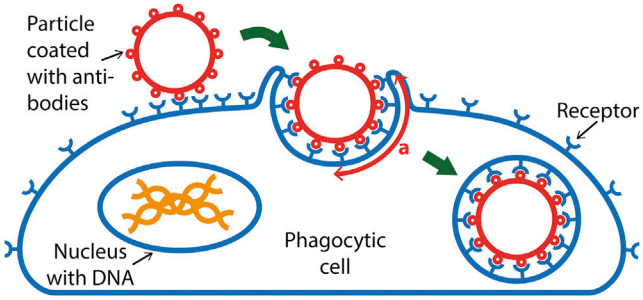

FIGURE 1 Phagocytosis of a target particle. Receptors on the cell surface bind ligand molecules on the target, such as a pathogen, dead cell, or bead. As receptors bind more and more ligand molecules, the cell membrane progressively engulfs the target. Upon full engulfment, a phagosome is formed, which fuses with lysosomes, leading to digestion of the target. We denote the arc length of engulfed membrane by a, which gradually increases during engulfment. To see this figure in color, go online.

boundary during engulfment, which increases as receptors flow toward the cup, now determined by the diffusion equation. Using this correspondence, it was shown that there exists an optimum particle size during endocytosis corresponding to the shortest engulfment time: particles both larger and smaller than this optimum size take longer to engulf. Although phagocytosis is considered a more active, more regulated process than endocytosis, it is quite possible that early events in phagocytosis are driven by passive processes and may share similarities with endocytosis.

In this article, we focus on the progression of engulfment, in particular on the rate of engulfment and its dependence on passive and active mechanisms. For a spherical bead with radius R, we define the engulfment, a, as the arc length from the center of the cup to the edge of the cup. At the start of phagocytosis, $a = 0$, with a then monotonically increasing during engulfment, reaching πR upon full engulfment (see Fig. 1). Naively, one might expect that a initially increases quickly (because membrane wrinkles are used to extend the membrane around the particle), followed by a slower stage as new membrane must be synthesized or brought from internal stores (19,20). Interestingly, we will find exactly the opposite. By analyzing multiple single-bead, single-cell movies, we find evidence for two distinct stages of engulfment: an initial slow stage followed by a much quicker second stage.

We then extend the passive endocytosis model of Gao et al. (18) to describe phagocytosis of spherical beads. Because phagocytosis of large particles is considered more active (for example, more actin-dependent) than endocytosis, we then expand this model to include processes such as receptor drift and signaling, finding good agreement with the experimental data. We then examine the effect of ligand density on the engulfment time, predicting that particles with intermediate density are engulfed quickest. Finally, we study how ellipsoidal particles are engulfed, providing a potential explanation for why such particles are more likely to be engulfed when the highly-curved tip is presented to the cell first.

MATERIALS AND METHODS

Phagocytosis movies

We studied six movies, four using 4.6-μm-diameter beads and two using 6.2-μm-diameter beads. Briefly, polystyrene beads were incubated first in BSA (bovine serum albumin) and then with rabbit anti-BSA antibody. Human neutrophils and beads were then picked up in separate micropipettes and brought into contact. Upon adhesion, the bead was released and phagocytosis observed under a bright-field microscope using a 63× objective. The aspiration pressure was continually adjusted to ensure the length of cell within the micropipette was constant. Because only a small part of the cell is within the pipette, we believe that this continual pressure adjustment is unlikely to effect phagocytosis. This is confirmed by previous work that uses the same setup (14,21,22). For details, see Herant et al. (23).

Image analysis

For each frame of a movie, the cell, bead, and pipette were automatically identified. Initially edge detection, using the Sobel method, was performed, after which the bead was found by using a Hough transform. This identified the center and radius of the bead in each frame. The pipette was identified by searching for a set of horizontal lines, capped by a vertical line (as in Fig. 2 *B*). Due to the phagocytic cup, the cell is not well described by a sphere. However, it was still possible to find the body of the cell (the cell minus the cup) by assuming the body was spherical. After removing the bead, pipette, and cell body from each frame, all that remained is the phagocytic cup, which was separated from the background by imposing a threshold. Finally we measured the size of the phagocytic cup, defined as the arc length of bead circumference bound to the cell membrane. For full details, see the Supporting Material.

Data fitting

We scanned through a discretized version of parameter space that was described by

$$A_1, A_2 = \{0.05,\ 0.1,\ 0.15, \ldots,\ 5.0\},$$

$$\alpha_1, \alpha_2 = \{0.05,\ 0.1,\ 0.15, \ldots,\ 1.5\},$$

$$t_0, t_1 = \{0,\ 1,\ 2, \ldots,\ T\},$$

where T is the total length of the movie and $t_0 < t_1$. For each point in this space, we define the error as

$$\sum_i (a_i - \overline{a}_i)^2,$$

where a_i is the measured engulfment from frame i, $\overline{a}_i$ is given by Eq. 1 applied at $t = t_i$, and the sum runs over all frames. The minimum error gives the best fit to the measured data. To test that the difference between the α_1 and α_2 distributions is statistically significant, we used the Mann-Whitney U-test, a nonparametric test often used for nonnormally distributed data, finding significance with $p < 0.02$ ($U = 107.5$, $n_{\alpha_1} = n_{\alpha_2} = 12$).

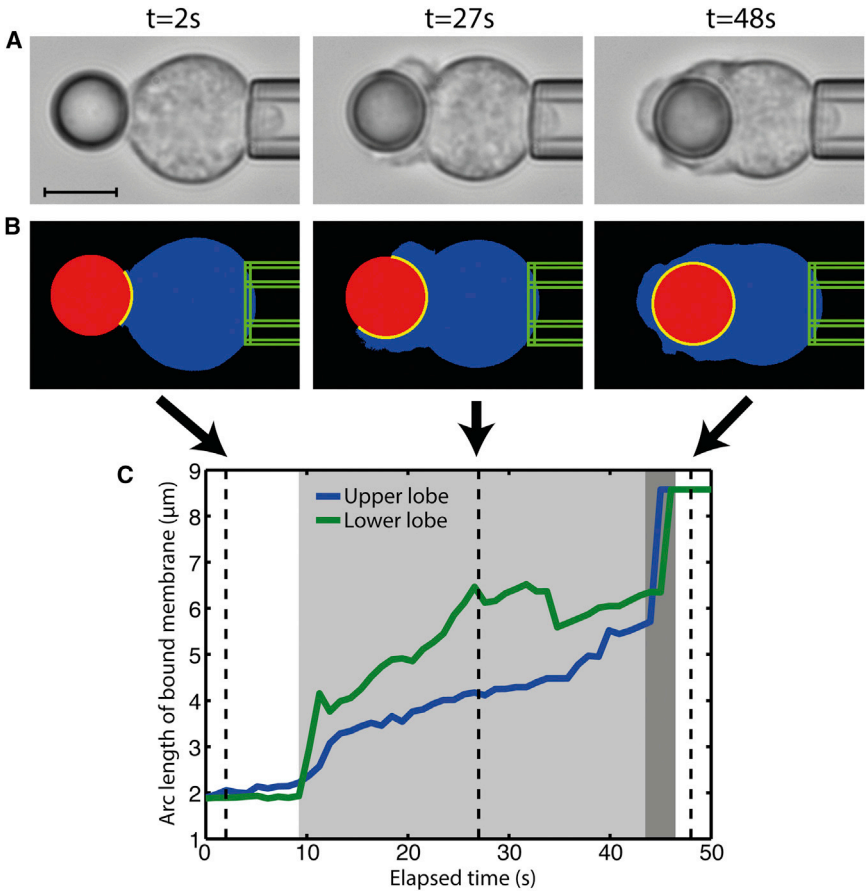

FIGURE 2 Typical time-lapse movie and image analysis of neutrophil engulfing an IgG-coated bead. Here the bead has diameter 4.6 μm. Data from Herant et al. (14). (*A*) Raw images of three frames at various stages of engulfment. At t ≈ 2 s, the bead has been released onto the cell, with a contact area of a ≈ 2 μm. At this point engulfment has not yet started. At t ≈ 27 s, the bead is approximately half-engulfed, with the lower lobe noticeably ahead of the upper lobe. At t ≈ 48 s, engulfment is complete, the bead is entirely within the cell, and the phagosome is fully formed. Scale bar: 5 μm. (*B*) The same frames as in panel *A* after automatic image analysis. (*Blue*) Cell; (*red*) bead; (*green*) outline of the pipette; (*yellow*) membrane attached to the bead. (*C*) Engulfment as a function of time. For both the upper and lower lobes, after engulfment begins at t ≈ 10 s, there is an initial slow stage (*light gray*) followed by a much quicker second stage (*dark gray*). Engulfment is complete by t ≈ 46 s. To see this figure in color, go online.

Numerical simulations

The diffusion-and-drift model and the model with signaling were solved numerically as follows. The membrane was represented by a finite grid of length $L = 50$ μm and spacing $\Delta r = 0.01$ μm, labeled by i. Given the values of $\rho_i(t)$, $S_i(t)$, and $a(t)$ at some time t, the values at the next time step, $t + \Delta t$ ($\Delta t = 2.5 \times 10^{-5}$ s), were found from the Euler method and by imposing the boundary condition $\rho_{i(a)}(t + \Delta t) = \rho_+$, where $i(a)$ is a expressed as an integer number of lattice steps and ρ_+ is found by solving Eq. 4. As a check of the numerical method and to ensure that values of Δr and Δt were sufficiently small, we checked that the numerical and analytic solutions matched for the pure diffusion and pure drift models. We also checked that decreasing Δr and Δt did not noticeably change the results, indicating convergence. See the Supporting Material for full details.

Parameter values

Parameter values were chosen as follows:

- $D = 1$ μm^2 s^{-1}, close to the Fcγ receptor diffusion constant reported in van Zon et al. (16);
- $v = 0.1$ μm s^{-1}, chosen so that engulfment after 1 min is similar in the pure diffusion and pure drift models;
- $\rho_0 = 50$ μm^{-2}, typical receptor density (18,24);
- $\rho_L = 500$ μm^{-2}, typical ligand density (25);
- $\varepsilon = 15$, measured FcγR-IgG binding free energy (15 k_BT) (26);
- $\beta = 20$, typical value of bending modulus (20 k_BT) (27);
- $R = 2$ μm, similar radius to the beads in our data; and
- $L = 50$ μm, approximate circumference of our cells.

RESULTS

Phagocytosis proceeds in two stages

We analyzed six time-lapse movies of FcγR-mediated neutrophil phagocytosis, four with beads of 4.6-μm diameter and two with beads of 6.2-μm diameter (one of which is published in Herant et al. (14)). Example frames are shown in Fig. 2 *A*. These were obtained by holding IgG-coated beads and neutrophils in separate micropipettes, before bead and cell were brought into contact and released. Image analysis was performed automatically to remove any human bias. Briefly, we used a combination of edge detection and Hough transforms to identify the position and size of the cell, bead, and pipette. After removing the bead, a threshold was applied, allowing the shape of the membrane engulfing the bead to be identified, from which the arc length of membrane engulfing the cell was calculated. For full details, see Materials and Methods. Examples of this analysis are shown in Fig. 2 *B*; see also Movie S1 in the Supporting Material.

In our focal plane we can identify two lobes of the phagocytic cup, which we refer to as the top and bottom (Fig. 2 *A*). Although the top and bottom lobes are connected, we analyzed them separately. Fig. 2 *C* shows a typical result of the engulfed arc length as a function of

time, with the remaining plots shown in Fig. S1 in the Supporting Material. Initially, there is a period (0–10 s in Fig. 2 *C*) when the bead is in contact with the cell, although engulfment has not started. This results in a nonzero, approximately constant contact length between the bead and cell, due to adhesion between them. At some point (~10 s in Fig. 2 *C*), engulfment begins and the engulfed arc length starts to increase as a function of time. Initially, this engulfment is relatively slow, with the rate of further engulfment decreasing in time. However, at some point (~44 s in Fig. 2 *C*) there is a sharp and rapid increase in engulfment rate, with full engulfment occurring soon after (~46 s in Fig. 2 *C*). These two stages of engulfment, an initial slow stage followed by a rapid second stage, occurred for both 4.6- and 6.2-μm beads. Surprisingly, engulfment in the slow stage proceeds at different rates in the top and bottom lobes. This suggests that, at least initially, engulfment is a local process, depending only on the distribution of receptors at a given point on the membrane.

Power laws describe engulfment

To test the idea of two distinct stages, we fit our data to a general two-step model by assuming that each stage is described by an independent power law. To this end, we describe the engulfed arc length, $a(t)$, in four parts (Fig. 3 *A*):

1. After the bead initially makes contact with the cell, there is a time when the bead sits on the surface of cell, with some nonzero engulfment, a_0.
2. After some time t_0, engulfment begins and the first, slower stage starts. We describe this using a power law, $a(t) \sim A_1 t^{\alpha_1}$, shifted so that $a = a_0$ at $t = t_0$.
3. At time t_1 when the engulfment is a_1, the second, faster stage is initiated, described by an independent power law, $a(t) \sim A_2 t^{\alpha_2}$, this time shifted so that $a = a_1$ at $t = t_1$.
4. At time t_2, the bead is completely engulfed and the engulfed arc length reaches its maximum of a_2.

Thus we model the engulfed arc length, where $a_1 = a_0 + A_1(t_1 - t_0)^{\alpha_1}$ and $a_2 = a_1 + A_2(t_2 - t_1)^{\alpha_2}$, as

$$a(t) = \begin{cases} a_0 & \text{for } t<t_0, \\ a_0 + A_1(t - t_0)^{\alpha_1} & \text{for } t_0 \le t<t_1, \\ a_1 + A_2(t - t_1)^{\alpha_2} & \text{for } t_1 \le t<t_2, \\ a_2 & \text{for } t \ge t_2. \end{cases} \quad (1)$$

We observed that a_0, the initial contact between the bead and cell, is approximately constant in all our movies, even for different bead sizes, with an average and standard deviation of $a_0 = 2.10 \pm 0.20$ μm. Thus, to reduce the number of parameters in the general model, we set $a_0 = 2.10$ μm from now on. Further, a_2, the arc length of membrane wrapping the bead at full engulfment, can readily be determined by examining the final few frames of each movie, after engulfment is complete. Thus, for any given movie, there are only six parameters to fit: the times t_0, t_1, the powers α_1, α_2, and the prefactors A_1, A_2 (see Materials and Methods for details).

The change from the slow to fast stage of engulfment occurs when the average fraction of bead engulfed is 0.47 ± 0.10, suggesting that the fast stage may be triggered at approximately half-engulfment when further engulfment requires the purse-string-like closure of the membrane around the bead (28). To examine the relative speeds of the first and second stages, we consider the fraction of total engulfment time spent in the first stage compared to that in the second, finding an average of 0.77 ± 0.15. This means that, on average, the first stage lasts more than three times longer than the second stage, despite the fact that both stages engulf approximately half the total bead area. In addition to this, the parameters α_1 and α_2 give information about the exact manner in which engulfment proceeds during each stage. We find that the median of α_1 is 0.68 whereas that of α_2 is 1.0 (see Fig. 3 *B* for medians and upper and lower quartiles), suggesting that the stages may be governed by entirely different processes.

We can also examine whether there are differences in engulfment between our two bead sizes. For the average total engulfment time, $t_2 - t_0$, we find, as expected, that

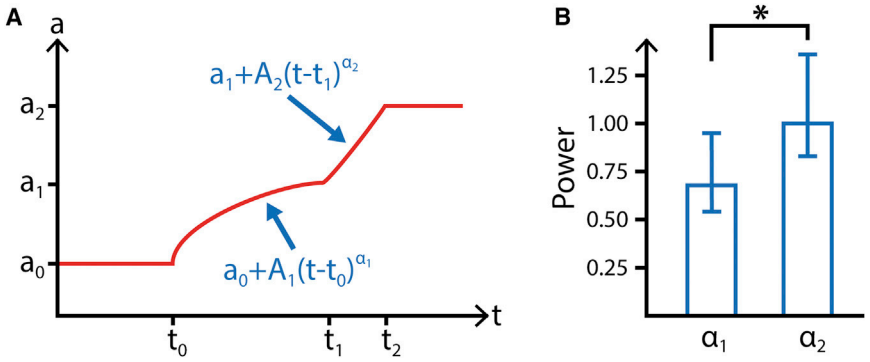

FIGURE 3 Fitting to the general model. (*A*) The general two-stage model is split into four regions. First, before engulfment begins, the contact length is constant with $a = a_0$. Second, after engulfment begins at $t = t_0$, the engulfed arc length is given as a power law with power α_1 and prefactor A_1. Third, after $t = t_1$, the second step begins and a is described by an independent power law with power α_2 and prefactor A_2. Fourth, after $t = t_2$, the particle is completely engulfed and $a = a_2$. (*B*) Comparison of the two powers, α_1 and α_2, showing the median and upper and lower quartiles. $n_{\alpha_1} = n_{\alpha_2} = 12$ (6 beads $\times$ 2 lobes). A Mann-Whitney U-test showed that the difference between α_1 and α_2 is significant ($p < 0.02$, $U = 107.5$). To see this figure in color, go online.

the larger beads take longer to engulf (37 ± 8 s for 4.6-μm beads and 90 ± 12 s for 6.2-μm beads). This relatively large increase is probably due to the available membrane becoming limiting for 6.2-μm beads, when the bead radius becomes similar to the cell radius. However, the fraction of bead engulfed at the start of the second stage is similar for both bead sizes (0.49 for 4.6-μm beads and 0.44 for 6.2-μm beads). Our data is insufficient to determine whether this small difference is significant. Finally, the change in α between the stages is again consistent for both radii (0.63 → 1.0 for 4.6-μm beads and 0.83 → 1.1 for 6.20-μm beads), suggesting that the two-stage mechanism is a general feature of phagocytosis, independent of bead size.

Pure diffusion model

To try to understand the possible origins of such different dynamics, we consider simple models, focusing mainly on the motion of the Fcγ receptors. Motivated by Gao et al. (18), we consider a circularly-symmetric two-dimensional membrane, with the origin being the point at which the bead first touches the cell. This is a reasonable assumption, given the spherical symmetry of the bead. The model describes aspects both of endocytosis (18) and of CR3-mediated phagocytosis where the bead normally sinks into the cell, as in Fig. 4 *A*. Even in Fcγ-mediated phagocytosis, where engulfment is by extension of the membrane around the bead (Fig. 4 *B*), the problem is still one of receptors moving in a two-dimensional membrane. Because in our simple model we neglect the details of the cup shape, the only relevant difference is that the total curvature is greater in the Fcγ-mediated case (although the local curvature is approximately the same, a greater area of membrane is curved). Thus, by including this extra curvature, we can also apply the same model to Fcγ-mediated phagocytosis (see the Supporting Material for details).

Due to the assumed circular symmetry, the problem reduces to receptors moving on a semi-infinite one-dimensional line. We parameterize this line by the distance from the origin, r, and describe the receptor density by $\rho(r,t)$, where t is the time. Before contact with any bead, the receptor density is independent of r and is given by ρ_0. During engulfment, the receptor distribution is no longer constant, although the density at infinity is always ρ_0. The second variable is the cup size, $a(t)$, the engulfed arc length measured from the center of the cup. Within the engulfed region, where $r < a$, receptors are attached to the ligands on the bead. As such, their density is assumed to be related to the ligand density on the bead and, for simplicity, we assume that ρ in this region is constant and given by ρ_L, where $\rho_L > \rho_0$. We denote the receptor density at the cup edge, $\rho(a(t),t)$, by $\rho_+(t)$. These variables and constants are shown in Fig. 4 *C*.

There are various possible physical mechanisms for the motion of the receptors in the nonengulfed region of the membrane, $r \geq a$. The first we consider is a purely passive process, where receptors simply diffuse around the membrane (18). Diffusion of ρ is then described by $\partial\rho/\partial t = D\nabla^2\rho$, where ∇^2 is the radial part of the Laplacian in cylindrical coordinates and D is the diffusion constant. The evolution of a is determined by conservation of receptors. Receptors move from outside to inside the cup region with flux $-D\rho'_+$, where ρ'_+ is shorthand for $\partial\rho/\partial r$, evaluated at $r = a$. This flux increases the density of receptors in the boundary region from ρ_+ to ρ_L, from which the rate of change of a follows. See the Supporting Material for details. Thus, our pure diffusion model, for the nonengulfed region of the membrane (where $r \geq a$), which is identical to the (supercooled) one-dimensional Stefan problem, is described by

$$\frac{\partial\rho}{\partial t} = \frac{D}{r}\frac{\partial}{\partial r}\left(r\frac{\partial\rho}{\partial r}\right), \tag{2a}$$

$$\frac{da}{dt} = \frac{D\rho'_+}{\rho_L - \rho_+}, \tag{2b}$$

with initial conditions $\rho(r,0) = \rho_0$ and $a(0) = 0$.

To find a solution to this system, one extra condition is needed. Following Gao et al. (18), we require that there is

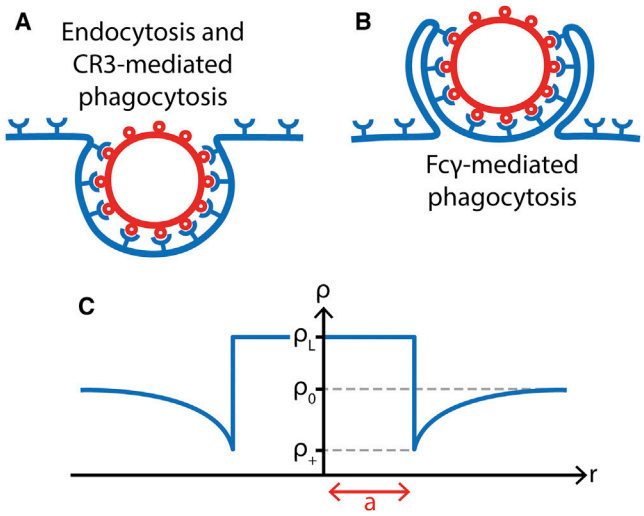

FIGURE 4 Types of phagocytosis and the model variables. (*A*) In CR3-mediated phagocytosis, the particle sinks into the cell, in a manner similar to endocytosis. (*B*) In contrast, in Fcγ-mediated phagocytosis, the membrane extends via pseudopod extensions outwards around the particle. Despite these differences, we believe that the movement of receptors within the membrane is similar in both cases, and can be described by the same simple model. (*C*) Sketch of the receptor density, ρ, which depends only on the distance from the center of the cup, r, and the time, t. Within the cup, which has arc length a, the receptor density is always fixed at ρ_L, whereas the density at infinity, which is the same as the initial density, is ρ_0. At the edge of the cup, the receptor density is fixed at ρ_+, which is calculated by considering the free energy. In the pure diffusion model, ρ_+ is always less than ρ_0, so that receptors always flow in toward the cup and increase the cup size. To see this figure in color, go online.

no free-energy change as receptors move into the engulfed region and the cup boundary is extended, indicating that all energy from receptor-ligand binding and configurational receptor entropy is used for bending the membrane and engulfment. We consider three contributions to the free energy: 1), the binding between receptors and ligands, 2), the curvature of the membrane, and 3), the receptor entropy. The negative energy from binding is necessary to cancel the positive contribution from membrane curvature. As explained in the Supporting Material, we can write the free energy, $\mathscr{F}$, as

$$\frac{\mathscr{F}}{2\pi k_B T} = \int_0^a \left(-\rho_L \mathscr{E} + \frac{1}{2}\mathscr{B}\kappa_p^2 \right) r dr + \int_0^\infty \rho \ln\left(\frac{\rho}{\rho_0}\right) r dr, \tag{3}$$

where $\mathscr{E}$ is the binding energy per receptor-ligand bond, $\mathscr{B}$ is the bending modulus, and κ_p is the radius of curvature of the bead. Although we do not explicitly include the membrane tension, such a term could be absorbed into the definition of $\mathscr{E}$ (see the Supporting Material). For a spherical bead of radius R, $\kappa_p = 2/R$. Requiring no free-energy jump across the cup boundary implies that

$$\frac{\rho_+}{\rho_L} - \ln\left(\frac{\rho_+}{\rho_L}\right) = \mathscr{E} - \frac{\mathscr{B}\kappa_p^2}{2\rho_L} + 1, \tag{4}$$

from which it follows that ρ_+, the receptor density at the cup edge, is a constant, independent of time. The (numerical) solution for ρ_+ gives the extra condition needed to uniquely solve the system (Eq. 2).

The solution, shown in Fig. 5 *A*, is then given by

$$\rho(r,t) = \begin{cases} \rho_L & \text{for } r<a, \\ \rho_0 - AE_1\left(\dfrac{r^2}{4Dt}\right) & \text{for } r \geq a, \end{cases} \tag{5a}$$

$$a(t) = 2\alpha\sqrt{Dt}, \tag{5b}$$

where

$$E_1(x) = \int_x^\infty \frac{e^{-u}}{u} du$$

is the exponential integral. As explained in the Supporting Material, the constant α is found by solving (numerically)

$$\alpha^2 e^{\alpha^2} E_1(\alpha^2) = \frac{\rho_0 - \rho_+}{\rho_L - \rho_+}, \tag{6}$$

after which A is given by $A = (\rho_0 - \rho_+)/E_1(\alpha^2)$. The most important property of the solution is the behavior of a, which increases as the square-root of time, $a \propto \sqrt{t}$. This is similar to the behavior we found when fitting the first stage of our movie data to the general model, suggesting that the first stage is controlled by passive receptor diffusion and capture.

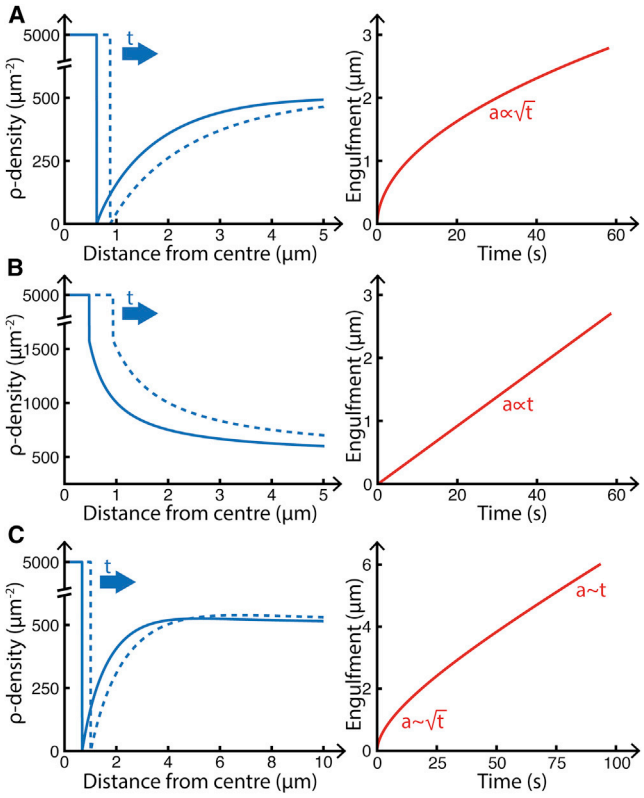

FIGURE 5 Results from the pure diffusion, pure drift, and diffusion-and-drift models. (*Left*) Receptor density profile. (*Right*) Engulfment against time. (*A*) Pure diffusion model with $D = 1\ \mu m^2\ s^{-1}$. The receptor density, ρ, drops significantly just outside the cup so that $\rho_+ < \rho_0$ and evolves to the right as engulfment proceeds. Note that the parameters are such that $\rho_+ \approx 0$. The engulfment increases as the square-root of time. Receptor profile shown at $t = 3$ s (*solid*) and $t = 6$ s (*dashed*). (*B*) Pure drift model with $v = 0.1\ \mu m\ s^{-1}$. The receptor density has a completely different profile and decreases away from the cup, with ρ_+ now greater than ρ_0. Importantly, the engulfment now increases linearly in time. Receptor profile shown at $t = 10$ s (*solid*) and $t = 20$ s (*dashed*). (*C*) Diffusion and drift model with $D = 1\ \mu m^2\ s^{-1}$ and $v = 0.1\ \mu m\ s^{-1}$. Engulfment now proceeds as a mixture of the pure diffusion and pure drift cases. Initially, when the receptor density is low, $a \sim \sqrt{t}$ as in the pure diffusion model. At later times, when the receptor gradient near the cup becomes approximately constant, a becomes more linear in time and behaves more like the pure drift result. Receptor profile shown at $t = 3$ s (*solid*) and $t = 6$ s (*dashed*). Parameters are $\rho_0 = 50\ \mu m^{-2}$, $\rho_L = 5000\ \mu m^{-2}$, $\mathscr{E} = 15$, $\mathscr{B} = 20$, $R = 2\ \mu m$, and $L = 50\ \mu m$. To see this figure in color, go online.

Pure drift model

In contrast to this purely diffusive, passive model, we now consider the other extreme: a model where receptors are actively moved toward the edge of the cup. To do this, we remove any diffusion and instead impose that the receptors drift with constant velocity toward the boundary $r = a$, requiring some active centripetal force, such as movement of receptors via retrograde actin flow (29). The movement of the receptors is now described by $\partial\rho/\partial t = v\nabla_r \cdot \rho$, where $\nabla_r \cdot$ only includes the radial part of the divergence in cylindrical coordinates and v is the drift velocity. The equation

for a is also changed because now the flux across the cup boundary is $-v\rho_+$. Thus, our second model (which is also a type of Stefan problem, but with diffusion replaced by drift) is given by

$$\frac{\partial \rho}{\partial t} = \frac{v}{r}\frac{\partial}{\partial r}(r\rho), \tag{7a}$$

$$\frac{da}{dt} = \frac{v\rho_+}{\rho_L - \rho_+}, \tag{7b}$$

with the same initial conditions as before.

Unlike for the diffusion model, there is no need for the extra condition obtained from free-energy considerations. The analytic solution, shown in Fig. 5 *B*, is given by

$$\rho(r,t) = \begin{cases} \rho_L & \text{for } r<a, \\ \rho_0\left(1+\dfrac{vt}{r}\right) & \text{for } r \geq a, \end{cases} \tag{8a}$$

$$a(t) = \frac{1}{\sqrt{\rho_L/\rho_0}-1}vt. \tag{8b}$$

The receptor density at the edge is given by

$$\rho_+ = \sqrt{\rho_L \rho_0},$$

which means that, because Eq. 4 will not in general be satisfied, it is impossible to avoid a free-energy jump across the boundary in this model. In contrast to the diffusion model, the rate of engulfment is now linear in time, $a \propto t$, which suggests that the drift model is more appropriate for the second, faster stage of engulfment, where, on average, we found $\alpha_2 = 1.0$.

Combining diffusion and drift

The pure diffusion and pure drift models are extreme cases, where the receptors either diffuse or drift, but not both. It is far more realistic to allow both behaviors, which results in a system that looks like a combination of Eqs. 2 and 7. As for the pure diffusion model, we again consider the free energy and require that there is no energy jump across the cup. Despite the addition of drift, the resulting equation for ρ_+ is unchanged from Eq. 4, so that the receptor density at the cup is again constant, independent of time. See the Supporting Material for details.

Unlike the pure diffusion and pure drift cases, this model cannot be solved analytically. Instead, as explained in Materials and Methods, we numerically solved the system on a finite-grid membrane. An example of the output is shown in Fig. 5 *C*. Near the cup, the receptor profile looks similar to the pure diffusion case, with positive gradient so that diffusion (in addition to drift) causes receptors to flow across the boundary and increase the cup size. Further from the cup, the density increases beyond the value at infinity, ρ_0, before turning around and decreasing back toward ρ_0. As with the pure diffusion model, the engulfed arc length $a(t)$ initially grows as $\sqrt{t}$. This is because, at early times, the flow of receptors into the cup is dominated by the relatively large gradient of ρ. At later times, when $\partial\rho/\partial r$ decreases, drift is the dominant cause of receptor flow, and $a(t)$ grows linearly with time. Thus, the combined diffusion and drift model initially looks like pure diffusion, with later behavior more similar to pure drift.

A full model that captures both phases of engulfment

Although the diffusion and drift model displays $a \sim \sqrt{t}$ and $a \sim t$ regimes, it is clear that it cannot explain the sharp jump in Fig. 2 *C*. To progress further, we consider, in addition to the receptors, the role of signaling via a signaling molecule described by density S. Although phagocytosis in a real cell depends on many types of signaling molecules in complicated cascades, it is not unreasonable to assume that just one species will capture the essential manner in which signaling influences the receptor dynamics. For simplicity, we imagine that our signaling molecule only moves within the membrane, as happens for some small GTPases. Due to the circular symmetry of the system, the signaling molecule, as with the receptors, can be described as a function of the distance from the origin r and the time t, so that $S = S(r,t)$.

We assume that initially there are no signaling molecules and that S is produced with constant rate in response to receptor-ligand binding. As such, S is only produced within the cup region where $r < a$. To counteract the production, we also allow S to degrade everywhere with constant lifetime. Finally, we let S diffuse throughout the membrane with diffusion constant D_S, which is generically different to the receptor diffusion constant D. Thus the dynamics of S (as sketched in Fig. 6 *A*) are described by

$$\frac{\partial S}{\partial t} = \frac{D_S}{r}\frac{\partial}{\partial r}\left(r\frac{\partial S}{\partial r}\right) + \beta\rho_L\Theta(a-r) - \tau^{-1}S, \tag{9}$$

where $\Theta(x)$ is the Heaviside function, $\beta\rho_L$ is the binding rate, and τ is the lifetime. For full details, see the Supporting Material.

In order that the signaling molecule can influence engulfment, i.e., that S can actually signal, we need to couple S to the dynamics of ρ. There are several ways we could do this, although we focus on the case where the density of the signaling molecule influences the drift speed. This can lead to radically different types of engulfment. For example, if we assume $v = v_1 S$ for some constant v_1, it is possible to get accelerated cup growth as shown in Fig. 6 *B*. In such a model there is initially no signaling, and therefore no drift. However, as the signaling molecule density at the cup edge

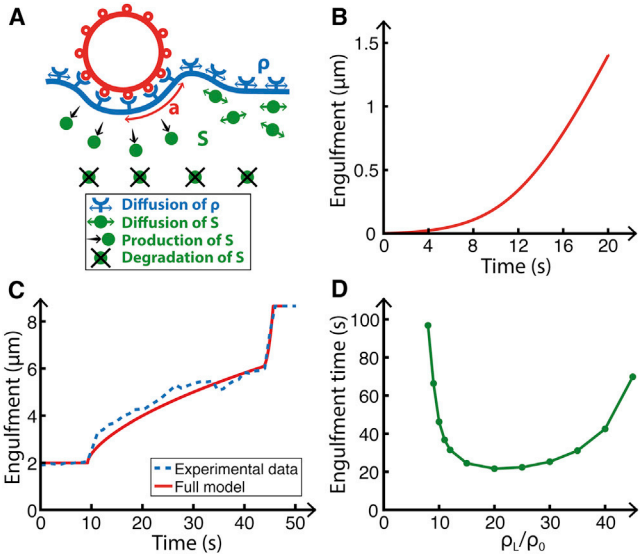

FIGURE 6 Engulfment model with signaling. (*A*) Sketch of the model which, in addition to the receptor density ρ, contains a signaling molecule with density S. Receptors can only diffuse (with diffusion constant D) and drift (with speed v), whereas the signaling molecule is produced within the cup with rate $\beta\rho_L$, degraded everywhere with lifetime τ, and diffuses with diffusion constant D_S. (*B*) In contrast to other models, the rate of engulfment can now accelerate if the drift velocity depends linearly on S via $v = v_1 S$, tending to a constant as $t \to \infty$. Parameters are $v_1 = 20\ \mu m^3\ s^{-1}$, $\beta = 0.1\ s^{-1}$, $\tau = 10$ s, and $R = 2\ \mu$m, no diffusion. (*C*) In the full model, with a drift velocity that depends on the signaling molecule via a threshold, S_0, and an initial latent period, t_0, a sharp increase in engulfment rate can be obtained, which matches well with the measured data. Here the measured data is the average of the upper and lower lobes for the 4.6-μm bead shown in Fig. 2 *C*. Parameters are $D = 3.8\ \mu m^2\ s^{-1}$, $v_1 = 6\ \mu m^3\ s^{-1}$, $S_0 = 0.498\ \mu m^{-2}$, $\beta = 0.4\ s^{-1}$, $\tau = 0.5$ s, $t_0 = 10$ s, and $R = 2.75\ \mu$m. (*D*) The dependence of the full-engulfment time on the ligand density, ρ_L, showing a minimum at intermediate ρ_L. Parameters as in panel *C*. Additional parameters are $\rho_0 = 50\ \mu m^{-2}$, $\mathscr{E} = 3$, $\mathscr{B} = 20$, $D_S = 1\ \mu m^2\ s^{-1}$, and $L = 50\ \mu$m. To see this figure in color, go online.

increases, the drift velocity also increases, leading to quicker and quicker engulfment.

The effect of signaling on the drift velocity is likely to be cooperative, with multiple signaling molecules required to activate drift. Although we could model this via Hill-like behavior with a large Hill coefficient, we instead choose, for simplicity, to use a threshold S_0. Receptors diffuse until the signaling molecule at the cup edge reaches S_0. At this point, constant drift is turned on at all positions. This model, as shown in Fig. 6 *C*, contains a rapid increase in the rate of engulfment when S_+ reaches S_0.

To complete our model we introduce an initial latent period of length t_0, representing the period when the particle sits on the cell, before engulfment begins. By fitting the model parameters, we obtain good agreement with our experimental data. For example, Fig. 6 *C* shows the fit with the data from the 4.6-μm bead shown in Fig. 2 *C* (averaged over the upper and lower lobes). Although simple, our model correctly captures the main features we observed during engulfment, including the two-stage behavior of the cup edge.

How engulfment depends on the ligand density

Using our full model, we now study the dependence of the engulfment time on the ligand density, ρ_L. This is not trivial because ρ_L appears in the cup growth rate (Eq. 2b), the receptor density at the cup edge (Eq. 4), and the production rate of the signaling molecule (Eq. 9). From our simulations we measure the full-engulfment time for various ρ_L (Fig. 6 *D*).

Interestingly, the behavior is not monotonic. For small ligand densities, the signaling molecule production rate is small and S only slowly increases toward S_0, leading to a long engulfment time. As ρ_L increases, this production rate increases, which tends to reduce the engulfment time. However, at the same time, the cup growth rate decreases (because more ligands must be bound), so that the region of S production ($r < a$) is smaller. This has the tendency to increase the engulfment time. These two competing effects lead to the nonmonotonic behavior, with an initial decrease before a final rise as ρ_L is increased. Notably, this predicts an optimum intermediate ligand density corresponding to the quickest possible engulfment. This is in sharp contrast to previous models (such as Gao et al. (18) and Decuzzi and Ferrari (30)), where the engulfment time monotonically increases with increasing ligand density (see Fig. S3 *E*). However, such models do not include signaling and neglect the two-stage nature of engulfment.

Although some previous experimental work has addressed the dependence of phagocytosis on ligand density (31,32), this usually involved measuring the percentage of engulfed particles, rather than the progression of the cup with time. This is more a measure of how often engulfment stalls, and is unlikely to be directly related to the engulfment rate. The engulfment time was measured in Zhang et al. (31), with similar cup closure times at different ρ_L. However, because only two ligand densities were studied, this does not conflict with our prediction, for which ligand densities either side of the optimum density can have similar engulfment times.

Ellipsoidal particles engulf quickest when presented tip-first

Finally, we study the effect of nonspherical particles. Because we are considering a one-dimensional model, our particles must be rotationally symmetric. For simplicity, we only consider spheroids—that is, ellipsoids where two of the principal axes have identical lengths. Thus spheroids are described by two parameters: R_1, the radius parallel to the membrane, and R_2, the radius perpendicular to the membrane (Fig. 7 *A*). The only difference from the above model is that κ_p in Eq. 4 is now $2H$, where H is the mean curvature

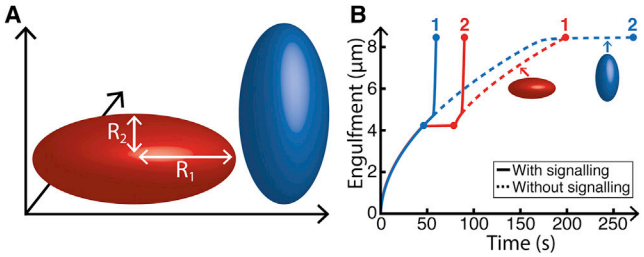

FIGURE 7 Comparison of oblate and prolate spheroids. (*A*) Sketch of the two spheroids, parameterized by R_1 and R_2. For oblate spheroids ($R_1 > R_2$), the lowest curvature region is the first to be engulfed, whereas for prolate spheroids ($R_1 < R_2$), the highest curvature region is engulfed first. (*B*) Progression of engulfment with time. (*Red*) Oblate spheroid with $R_1 = R_2 = 4.1$ μm and $R_3 = 0.62$ μm. (*Blue*) Prolate spheroid with $R_1 = R_2 = 0.87$ μm and $R_3 = 4$ μm. (*Solid lines*) Full model with signaling; (*dashed lines*) pure diffusion model without signaling. (*Solid circles*) Half- and full engulfment. (*Numbers*) Order of engulfment. To see this figure in color, go online.

of the spheroid. By using the standard parameterization of the surface of a spheroid,

$$\begin{aligned} x &= R_1 \sin v \cos u, \\ y &= R_1 \sin v \sin u, \\ z &= -R_2 \cos v, \end{aligned} \tag{10}$$

where $u \in [0,2\pi)$ and $v \in [0,\pi]$, we can write the mean curvature as (33)

$$2H = \frac{R_2\left[R_1^2(1+\cos^2 v) + R_2^2 \sin^2 v\right]}{R_1\left(R_1^2 \cos^2 v + R_2^2 \sin^2 v\right)^{3/2}}. \tag{11}$$

At any given time, we determine the value of v at the cup edge (corresponding to engulfed arc length a) and hence the curvature at $r = a$. This, via Eq. 4, gives the value of the receptor density at the cup edge, ρ_+. High curvature regions lead to relatively large values of ρ_+, and hence to slower engulfment.

Because we can only consider particles with two equal axes, we cannot directly compare the standing and lying-down versions of the same spheroid. Instead, we compare a spheroid where $R_1 > R_2$ (which is an oblate spheroid as in the first shape in Fig. 7 *A*) with a spheroid with $R_1 < R_2$ (which is a prolate spheroid as in the second shape in Fig. 7 *A*). To make the comparison meaningful, we ensure that both spheroids have the same circumference (i.e., the same total engulfment length). We also assume that these high-symmetry orientations are stable during engulfment.

To begin, we study the (unnatural) situation with signaling turned off, i.e., our pure diffusion model. For the oblate spheroid, the curvature is initially low, increasing to a maximum at half-engulfment, before decreasing back to its initial value. This leads to a fast-slow-fast type of engulfment, with the slowest cup progression occurring near half-engulfment (*red dashed curve* in Fig. 7 *B*). In contrast, for the prolate spheroid, the highest curvatures occur at the beginning and end of engulfment. In principle, this leads to slow-fast-slow engulfment, although the first stage is so short that it is better described as fast-slow engulfment (*blue dashed curve* in Fig. 7 *B*). Because the highest curvature region occurs toward the end in the prolate case, when the engulfment rate is already low, this has a much greater effect on cup progression, meaning that (without signaling) the prolate spheroid takes longer to engulf.

The situation, however, is markedly different for our full model with signaling (*solid curves* in Fig. 7 *B*). Although the prolate spheroid takes longer than the oblate spheroid to reach full engulfment, it reaches half-engulfment earlier. Consequently, the signaling molecule also reaches the threshold S_0 earlier, so that the second rapid engulfment stage begins sooner. Thus, with signaling, it is actually the prolate spheroid that is the first to complete engulfment. This agrees well with previous experimental observations, where nonspherical particles were found to be much easier to engulf when presented tip-first (34). A similar effect was observed in van Zon et al. (16), but in a model that ignores the two distinct stages of engulfment.

DISCUSSION

By analyzing time-lapse movies of neutrophils exposed to IgG-coated beads, we found evidence of two distinct stages during phagocytosis engulfment. The first stage proceeds relatively slowly, taking, on average, three-quarters of the total engulfment time to reach only half-engulfment. In contrast, engulfment is much quicker in the second stage, often only taking a few seconds. This is perhaps opposite to the expected behavior: the initial availability of spare membrane within membrane wrinkles might be thought to lead to quick initial engulfment, with a subsequent slowing as new membrane must be created or brought from internal stores (19,20). However, this argument can be turned on its head: perhaps it is precisely the need to create new membrane at approximately half-engulfment that is the signal for the cell to enter a second, more active phase of engulfment, with a rapid increase in engulfment speed.

This experimental observation seems to conflict with the result in Masters et al. (19), which also found two stages, but with an initial rapid stage followed by a slower second stage. However, Masters et al. (19) mostly involves macrophages spreading on a flat glass surface, whereas we study neutrophils engulfing spherical beads. This is likely to be substantially different both because of the huge difference in curvature (engulfment is highly dependent on curvature (18,34)) and, perhaps more importantly, because Masters et al. (19) necessarily involves frustrated phagocytosis, where engulfment can never complete. However, we believe the main difference occurs due to their large initial contact area, where cells placed on a glass surface instantly spread so that their initial contact area is ~140 μm^2 (see their Fig. 1 *B*), which is well above the total surface area for even our large 6.2-μm bead. Thus the

cells in Masters et al. (19) start with a contact area larger than that of complete engulfment for our beads, so that it seems likely that they may miss our initial slow stage when the cell is engulfing the first half of the target. Given this, the first stage in Masters et al. (19) should be identified with our second stage. It is perhaps also relevant that Masters et al. (19) used macrophages rather than neutrophils.

Motivated by the appearance of two stages, we then developed various models to describe engulfment. A complete mathematical model of phagocytosis is made difficult by the sheer number of parameters involved, which would in turn severely reduce its predictive power. Instead, we made progress by considering simplified models that only focus on the key components, ignoring the role of myosins, the need for cytoskeletal remodeling, and the full three-dimensional membrane shape. Motivated by the elegant model of endocytosis in Gao et al. (18), our simplest model only focused on the Fcγ receptors and assumed that the membrane appeared flat to the receptors. Although these are significant simplifications, we believe that our model still gives useful information about how the cell organizes phagocytosis and can correctly capture the basic receptor dynamics. By the addition of receptor drift and a signaling molecule, we were able to develop a full, yet still simple, model that captures the sharp jump in engulfment rate.

The switch to the second stage occurs, on average, at almost exactly half-engulfment, which is precisely the point when the cell must start to tighten the cup around the top-half of the particle for cup closure. This switch could provide an alternative explanation to the observation in van Zon et al. (16) that cells either fully engulf a target particle or stall before the half-way point. If, sometimes, perhaps due to insufficient signaling, the trigger for the second stage does not occur, this would leave cells at half-engulfment, without the necessary new membrane or modified receptor dynamics to enter the second stage and proceed to full engulfment.

How could the cell identify and signal the switch to the second stage of engulfment? Identification could be achieved in a variety of ways, perhaps by the increased membrane tension during engulfment (19), by the exhaustion of membrane wrinkles (20), or by the reduced speed of engulfment. With regard to signaling, various proteins are known to be expressed at later stages of engulfment and may therefore serve as the signal for the switch (3,31,35). For example, Rac1 and Rac2 (small signaling GTPases) localize to the cup well after engulfment begins, with Rac1 appearing first (36). Similarly, PKCε, a serine/threonine kinase, is only involved during the later stages of cup formation (37). Although originally thought to be important only when the phagosome is fully formed, it was shown in Zhang et al. (31) that PKCε reaches one-half its maximum signal well before cup closure. Because stalled cups do not recruit PKCε (31), this would also tally with PKCε playing some role during the second stage of engulfment. Finally, phosphatidylinositol 3-kinase has been shown to be required for phagosome contraction during the later stages of engulfment (38).

The second stage is markedly faster than the first. With engulfment described by a power law, $a \sim At^{\alpha}$, this increased engulfment rate could be achieved either by increasing the prefactor A, increasing the power α, or by a combination of both. Our fit to the data (and our full model) suggests an increase in the power ($\alpha_2 \gtrsim 1$), corresponding to the activation of drift in response to signaling (Fig. 6). Such active drift motion of receptors toward the cup could be achieved, for example, by coupling the receptors to centripetal actin dynamics as observed in immunological synapses (29). In addition, it is likely that actin plays a role during the second stage, perhaps mediated by myosin IC (28). The full model leads to an interesting prediction for the receptor density near the cup. As seen in Fig. 5, *A* and *B*, the switch from diffusion to drift causes the sign of the receptor density gradient to switch immediately outside the cup: the depletion seen near the cup in the first stage disappears during the second stage. It would be interesting to tag the Fcγ receptor and try to observe this. Further, and perhaps surprisingly, our model predicts that the quickest engulfment occurs for some intermediate value of the ligand density, a claim that would also be interesting to test. In addition, we found that our model can explain the observation that tip-first ellipsoids are easier to engulf. In fact, our model goes further and predicts the entire engulfment time course for such particles, a result that could also be tested, perhaps with the same micropipette assay used in Herant et al. (14).

Although our analysis favors an increase in the power α during the second stage, it is also possible that the cell implements the faster engulfment stage by increasing the prefactor A. This would still require active processes, but now the second stage would correspond to the pure diffusion model (as with the first stage), but with altered parameters. As explained in the Supporting Material, such behavior could be achieved either by increasing the receptor diffusion constant D, increasing the receptor-ligand binding strength $\mathscr{E}$, decreasing the bending strength $\mathscr{B}$, or by increasing the total number of receptors. Biologically these parameter changes could potentially be achieved by posttranslational modifications of the receptors, by receptor clustering (39), or by modifying the membrane structure (perhaps by altering lipid composition (40) or the connection with the actin cytoskeleton (41)). Models where the prefactor A increases would differ from those where the power α increases, because the receptor density would remain depleted just outside the cup even during the second stage. Thus, in principle, fluorescence microscopy of tagged receptors could distinguish between these two scenarios.

Understanding phagocytosis is of vital importance, given its crucial role in the immune system and its relevance to drug delivery (42). Despite the staggering molecular

complexity, simple physical mechanisms constrain and simplify the process, including membrane capacity (43), particle stiffness (44), and particle shape (34). Our simplified mathematical model shows that cells employ a multistage approach to engulfment, with radically different receptor dynamics occurring during different stages of engulfment. Potentially the second stage is a later evolutionary addition, resulting in increased engulfment speed and robustness. Conversely, such an approach may help overcome the difficulty of engulfing the final part of the target, or perhaps function as a means of first examining the particle, a way of checking the desirability and feasibility of engulfment, before fully committing the cell machinery to the engulfment process.

SUPPORTING MATERIAL

Additional supplemental information, three figures, and one movie are available at http://www.biophysj.org/biophysj/supplemental/S0006-3495(14)00845-5.

We thank Volkmar Heinrich for providing movies of phagocytosis, and Benoit Raymond, Marianne Guenot, and Gadi Frankel for useful discussions.

D.M.R. and R.G.E. were supported by Biotechnology and Biological Sciences Research Council grant No. BB/I019987/1. R.G.E. also acknowledges funding from European Research Council Starting Grant No. 280492-PPHPI.

SUPPORTING CITATIONS

References (45–51) appear in the Supporting Material.

REFERENCES

1. Flannagan, R. S., V. Jaumouillé, and S. Grinstein. 2012. The cell biology of phagocytosis. *Annu. Rev. Pathol.* 7:61–98.
2. Botelho, R. J., and S. Grinstein. 2011. Phagocytosis. *Curr. Biol.* 21:R533–R538.
3. Swanson, J. A. 2008. Shaping cups into phagosomes and macropinosomes. *Nat. Rev. Mol. Cell Biol.* 9:639–649.
4. Griffin, Jr., F. M., J. A. Griffin, …, S. C. Silverstein. 1975. Studies on the mechanism of phagocytosis. I. Requirements for circumferential attachment of particle-bound ligands to specific receptors on the macrophage plasma membrane. *J. Exp. Med.* 142:1263–1282.
5. Griffin, Jr., F. M., J. A. Griffin, and S. C. Silverstein. 1976. Studies on the mechanism of phagocytosis. II. The interaction of macrophages with anti-immunoglobulin IgG-coated bone marrow-derived lymphocytes. *J. Exp. Med.* 144:788–809.
6. McKenzie, S. E., and A. D. Schreiber. 1998. Fcγ receptors in phagocytes. *Curr. Opin. Hematol.* 5:16–21.
7. Joshi, T., J. P. Butchar, and S. Tridandapani. 2006. Fcγ receptor signaling in phagocytes. *Int. J. Hematol.* 84:210–216.
8. Nimmerjahn, F., and J. V. Ravetch. 2008. Fcγ receptors as regulators of immune responses. *Nat. Rev. Immunol.* 8:34–47.
9. Berton, G., A. Mócsai, and C. A. Lowell. 2005. Src and Syk kinases: key regulators of phagocytic cell activation. *Trends Immunol.* 26:208–214.
10. Diakonova, M., G. Bokoch, and J. A. Swanson. 2002. Dynamics of cytoskeletal proteins during Fcγ receptor-mediated phagocytosis in macrophages. *Mol. Biol. Cell.* 13:402–411.
11. Dart, A. E., S. Tollis, …, R. G. Endres. 2012. The motor protein myosin 1G functions in FcγR-mediated phagocytosis. *J. Cell Sci.* 125:6020–6029.
12. Underhill, D. M., and A. Ozinsky. 2002. Phagocytosis of microbes: complexity in action. *Annu. Rev. Immunol.* 20:825–852.
13. Metchnikoff, É. 1884. About anthrax bacilli on the relationship of phagocytes [Über die Beziehung der Phagocyten zu Milzbrandbacillen]. *Arch. Pathol. Anat.* 97:502–526.
14. Herant, M., V. Heinrich, and M. Dembo. 2006. Mechanics of neutrophil phagocytosis: experiments and quantitative models. *J. Cell Sci.* 119:1903–1913.
15. Herant, M., C.-Y. Lee, …, V. Heinrich. 2011. Protrusive push versus enveloping embrace: computational model of phagocytosis predicts key regulatory role of cytoskeletal membrane anchors. *PLOS Comput. Biol.* 7:e1001068.
16. van Zon, J. S., G. Tzircotis, …, M. Howard. 2009. A mechanical bottleneck explains the variation in cup growth during FcγR phagocytosis. *Mol. Syst. Biol.* 5:298.
17. Tollis, S., A. E. Dart, …, R. G. Endres. 2010. The zipper mechanism in phagocytosis: energetic requirements and variability in phagocytic cup shape. *BMC Syst. Biol.* 4:149.
18. Gao, H., W. Shi, and L. B. Freund. 2005. Mechanics of receptor-mediated endocytosis. *Proc. Natl. Acad. Sci. USA.* 102:9469–9474.
19. Masters, T. A., B. Pontes, …, N. C. Gauthier. 2013. Plasma membrane tension orchestrates membrane trafficking, cytoskeletal remodeling, and biochemical signaling during phagocytosis. *Proc. Natl. Acad. Sci. USA.* 110:11875–11880.
20. Hallett, M. B., and S. Dewitt. 2007. Ironing out the wrinkles of neutrophil phagocytosis. *Trends Cell Biol.* 17:209–214.
21. Lee, C. Y., M. Herant, and V. Heinrich. 2011. Target-specific mechanics of phagocytosis: protrusive neutrophil response to zymosan differs from the uptake of antibody-tagged pathogens. *J. Cell Sci.* 124:1106–1114.
22. Heinrich, V., and W. Rawicz. 2005. Automated, high-resolution micropipet aspiration reveals new insight into the physical properties of fluid membranes. *Langmuir.* 21:1962–1971.
23. Herant, M., V. Heinrich, and M. Dembo. 2005. Mechanics of neutrophil phagocytosis: behavior of the cortical tension. *J. Cell Sci.* 118:1789–1797.
24. Quinn, P., G. Griffiths, and G. Warren. 1984. Density of newly synthesized plasma membrane proteins in intracellular membranes II. Biochemical studies. *J. Cell Biol.* 98:2142–2147.
25. Gandour, D. M., and W. S. Walker. 1983. Macrophage cell cycling: influence on Fc receptors and antibody-dependent phagocytosis. *J. Immunol.* 130:1108–1112.
26. Raychaudhuri, G., D. McCool, and R. H. Painter. 1985. Human IgG1 and its Fc fragment bind with different affinities to the Fc receptors on the human U937, HL-60 and ML-1 cell lines. *Mol. Immunol.* 22:1009–1019.
27. Pontes, B., Y. Ayala, …, H. M. Nussenzveig. 2013. Membrane elastic properties and cell function. *PLoS ONE.* 8:e67708.
28. Swanson, J. A., M. T. Johnson, …, N. Araki. 1999. A contractile activity that closes phagosomes in macrophages. *J. Cell Sci.* 112:307–316.
29. Yu, C. H., H.-J. Wu, …, J. T. Groves. 2010. Altered actin centripetal retrograde flow in physically restricted immunological synapses. *PLoS ONE.* 5:e11878.
30. Decuzzi, P., and M. Ferrari. 2007. The role of specific and non-specific interactions in receptor-mediated endocytosis of nanoparticles. *Biomaterials.* 28:2915–2922.
31. Zhang, Y., A. D. Hoppe, and J. A. Swanson. 2010. Coordination of Fc receptor signaling regulates cellular commitment to phagocytosis. *Proc. Natl. Acad. Sci. USA.* 107:19332–19337.
32. Pacheco, P., D. White, and T. Sulchek. 2013. Effects of microparticle size and Fc density on macrophage phagocytosis. *PLoS ONE.* 8:e60989.

33. Weisstein, E. W. 2014. Ellipsoid. *MathWorld—A Wolfram Web Resource*. http://mathworld.wolfram.com/Ellipsoid.html. Accessed May 28, 2014.

34. Champion, J. A., and S. Mitragotri. 2006. Role of target geometry in phagocytosis. *Proc. Natl. Acad. Sci. USA.* 103:4930–4934.

35. Swanson, J. A., and A. D. Hoppe. 2004. The coordination of signaling during Fc receptor-mediated phagocytosis. *J. Leukoc. Biol.* 76:1093–1103.

36. Hoppe, A. D., and J. A. Swanson. 2004. Cdc42, Rac1, and Rac2 display distinct patterns of activation during phagocytosis. *Mol. Biol. Cell.* 15:3509–3519.

37. Larsen, E. C., T. Ueyama, …, M. R. Lennartz. 2002. A role for PKC-ε in FcγR-mediated phagocytosis by RAW 264.7 cells. *J. Cell Biol.* 159:939–944.

38. Araki, N., M. T. Johnson, and J. A. Swanson. 1996. A role for phosphoinositide 3-kinase in the completion of macropinocytosis and phagocytosis by macrophages. *J. Cell Biol.* 135:1249–1260.

39. Sobota, A., A. Strzelecka-Kiliszek, …, K. Kwiatkowska. 2005. Binding of IgG-opsonized particles to Fcγ R is an active stage of phagocytosis that involves receptor clustering and phosphorylation. *J. Immunol.* 175:4450–4457.

40. Mercanti, V., S. J. Charette, …, P. Cosson. 2006. Selective membrane exclusion in phagocytic and macropinocytic cups. *J. Cell Sci.* 119:4079–4087.

41. Andrews, N. L., K. A. Lidke, …, D. S. Lidke. 2008. Actin restricts FcεRI diffusion and facilitates antigen-induced receptor immobilization. *Nat. Cell Biol.* 10:955–963.

42. Lin, S.-Y., W.-H. Hsu, …, G.-H. Hsiue. 2011. Novel geometry type of nanocarriers mitigated the phagocytosis for drug delivery. *J. Control. Release.* 154:84–92.

43. Cannon, G. J., and J. A. Swanson. 1992. The macrophage capacity for phagocytosis. *J. Cell Sci.* 101:907–913.

44. Beningo, K. A., and Y. L. Wang. 2002. Fc-receptor-mediated phagocytosis is regulated by mechanical properties of the target. *J. Cell Sci.* 115:849–856.

45. Gonzalez, R., and R. Woods. 2007. Digital Image Processing. Prentice Hall, Upper Saddle River, NJ, pp. 728–736.

46. Duda, R. O., and P. E. Hart. 1972. Use of the Hough transformation to detect lines and curves in pictures. *Commun. ACM.* 15:11–15.

47. Helfrich, W. 1973. Elastic properties of lipid bilayers: theory and possible experiments. *Z. Naturforsch. C.* 28:693–703.

48. Freund, L. B., and Y. Lin. 2004. The role of binder mobility in spontaneous adhesive contact and implications for cell adhesion. *J. Mech. Phys. Solids.* 52:2455–2472.

49. Myers, T. G., S. L. Mitchell, and F. Font. 2012. Energy conservation in the one-phase supercooled Stefan problem. *Int. Commun. Heat Mass.* 39:1522–1525.

50. Chadam, J., and P. Ortoleva. 1983. The stability effect of surface tension on the development of the free boundary in a planar, one-dimensional, Cauchy-Stefan problem. *IMA J. Appl. Math.* 30:57–66.

51. Dewynne, J. N., S. D. Howison, …, W. Xie. 1989. Asymptotic behavior of solutions to the Stefan problem with a kinetic condition at the free boundary. *J. Austral. Math. Soc. Ser. B.* 31:81–96.

Supporting Material for *The mechanism of phagocytosis: two stages of engulfment*

David M. Richards[1,2], Robert G. Endres[1,2]

[1] Department of Life Sciences, Imperial College, London, UK
[2] Centre for Integrative Systems Biology and Bioinformatics, Imperial College, London, UK

1 Details of image analysis

For any given movie, we studied one frame at a time and attempted to identify the bead, cell and pipette. This was made easier by first performing edge detection using the Sobel method with a constant threshold (1). We found that the best results were obtained by manually tuning this threshold for each movie.

For a given frame i, we first tried to identify the bead by assuming it to be spherical, so that it appeared as a circle in cross section and could be defined by a triplet containing its centre and radius (x_i, y_i, r_i). Here x_i, y_i and r_i are measured in pixels. To search for the bead we considered the three-dimensional Hough space of all possible bead positions and radii (2). Since the bead only moves a few pixels between frames and has approximately constant shape, we narrowed the search by only considering a Hough space in the neighbourhood of the bead in the previous frame. So, for frame i we considered a Hough space $\mathcal{H}$ consisting of points (x, y, r) with $x \in [x_{i-1} - L_x, x_{i-1} + L_x]$, $y \in [y_{i-1} - L_y, y_{i-1} + L_y]$ and $r \in [r_{i-1} - L_r, r_{i-1} + L_r]$. We used $L_x = L_y = 10$px and $L_r = 2$px, although we checked that other values made little difference. For each point in $\mathcal{H}$, which describes a particular candidate circle, we calculated a score based on the number of pixels in the frame that overlapped with the candidate circle. Each pixel that overlapped contributed $1/r$ to the score. This inverse scaling with radius ensured that larger circles (with larger circumferences) were not more likely to be identified. After determining the score for each point in the Hough space, the maximum over all $\mathcal{H}$ gave the most likely position and radius of the bead.

A similar procedure was used to identify the pipette, which was idealised as a series of horizontal lines, capped by a vertical line on the right (see Fig. 2 in the main text). Since a horizontal (or vertical) line is described by only one parameter, its distance from the x (or y) axis, the Hough space was now only one-dimensional. Because the pipette consists of several horizontal lines, we

searched for several local maxima of $\mathcal{H}$ rather than the absolute maximum. To avoid finding local maxima with very low scores we imposed a threshold: ignoring maxima with scores less than 10% of the absolute maximum score was found to accurately identify the pipette.

Identifying the cell was potentially more difficult since, especially during engulfment, the cell is not spherical. However, we accounted for this by modelling the cell as a spherical part (which appeared as a circle in cross section) with protrusions on the left surrounding the bead. By first searching for circles with the same procedure as we searched for the bead, it was possible to identify the spherical part of the cell after which we defined the position and radius of the cell as the position and radius of the spherical part. Since the cell radius changes more (and faster) than that of the bead, we used $L_x = L_y = 5$ for the cell.

For both the bead and the spherical part of the cell, we also tried fitting ellipsoids (ellipses in cross section) rather than spheres. This made the Hough space five-dimensional: the x and y positions of the centre, the major and minor axes, and the orientation. However, despite the added complexity, there was no improvement in the bead and cell identification and no improvement in the measure of the engulfment.

After the bead, pipette and spherical portion of the cell were identified they were removed from the frame. This just left the background and the phagocytic cup. By imposing a threshold it was possible to separate the cup from the background and hence measure the arc length of the engulfed region. Choosing the correct threshold was critical for correctly identifying the edge of cup and so its value was set by hand for each movie.

2 Mathematical model of phagocytosis

Our pure diffusion model is identical to that in (3), although we apply the model to phagocytosis rather than endocytosis. We then extend this model in two ways: firstly to include drift, by adding non-diffusive receptor dynamics, and secondly by adding a second species, a signalling molecule, that interacts with the receptors.

2.1 Applicability to phagocytosis

Superficially it might appear that the model of endocytosis in (3) is not relevant to phagocytosis. The "sinking" of a particle into the cell during endocytosis (Fig. S2A) is in marked contrast to the protrusions that surround the target in Fcγ-mediated phagocytosis (Fig. S2B–C). However, our model

is sufficiently simple that this is unlikely to make a significant difference. As described below, we focus only on the Fcγ receptors (and later the signalling molecules) and their motion within the membrane. The receptor does not "feel" the curvature of the surface directly and so cannot distinguish the case where the membrane sinks inwards to that where the membrane protrudes outwards.

We do include the curvature of the membrane, but only, as explained below, as part of the free energy (the membrane bending term). Since the membrane must bend back on itself in Fcγ-mediated phagocytosis, the curvature is clearly greater than in endocytosis. However, this is easily accounted for by increasing the membrane bending contribution. Although the real cup shape is likely to be complicated, we consider two limits that are both easily incorporated into our model: an infinitely thin cup (Fig. S2B) and a symmetric cup (Fig. S2C). In both cases the membrane bound to the target (in orange in Fig. S2) has the same arc length and curvature as the rest of the cup (green in Fig. S2). Thus the area of curved membrane is four times larger (due to a doubling of the arc length). Since, as explained below, the bending energy is proportional to $\mathcal{B}A$, where $\mathcal{B}$ is the bending modulus and A the area, a four times increase in area can equivalently be interpreted as a four times increase in bending modulus. This means that we can incorporate the difference between endocytosis and phagocytosis simply by replacing $\mathcal{B}$ by $4\mathcal{B}$. It is worth noting that this analysis neglects the high curvature from the cup rims. This is unlikely to significantly effect our results, especially since the free-energy contribution from such regions may well be reduced by specific lipids with intrinsically high curvature.

2.2 General model setup

We consider receptors, described by a density ρ, moving in an infinite 2D membrane. Using an infinite membrane allows us to obtain analytic solutions and, as long as the surface area of the bead is sufficiently small compared to the membrane area, the infinite-membrane solutions are similar to the finite-membrane solutions. When we perform numerical simulations we, of course, use finite membranes. Although the membrane is curved, we assume that, from the point of the view of the receptors (which move only within the membrane), the membrane can be described as flat. We parameterise this surface by 2D polar coordinates, r and θ, where the origin is the point where the bead first makes contact with the cell. Since we only consider engulfment of spherical beads and deterministic models, we expect ρ (and the position of the edge of the cup) to be circularly symmetric and so the θ coordinate plays no role. So the problem is effectively formulated in only one space dimension,

r, the distance from the centre of the cup. Since we are interested in how quantities change in time, we consider $\rho(r,t)$. Before the start of engulfment we assume that, due to diffusion, the receptors are evenly distributed over the membrane, with constant density ρ_0, so that $\rho(r,0) = \rho_0$. Further, we assume that the receptor density at spatial infinity always remains at ρ_0 so that $\lim_{r\to\infty} \rho(r,t) = \rho_0$ for all t.

The second variable in our models, besides ρ, is the arc length of the engulfed membrane (equivalently the arc length of the engulfed region of the bead), which we label $a(t)$. The engulfed area, A, is related to a by $A = 2\pi R^2 \left(1 - \cos\left(\frac{a}{R}\right)\right)$, which is the surface area of a spherical cap, where R is the radius of the bead. For simplicity we assume that initially there is no engulfment, *i.e.* $a(0) = 0$. (In practice there is always some initial "engulfment" due to adhesion between the bead and the cell.) As engulfment proceeds, $a(t)$ increases with time, until full engulfment when $a = \pi R$. We assume some type of ratchet mechanism (4), where a can never decrease, *i.e.* $a(t)$ is monotonically increasing in time. Within the engulfed region, where $r < a$, we assume that the receptor density is fixed at ρ_L (with $\rho_L > \rho_0$). This is because we assume receptors in this region are attached to ligands on the beads, so that their density is set by the ligand density. As such we do not consider receptor dynamics within the engulfed region. An important quantity is the receptor density at the edge of the cup, where $r = a$, which we label ρ_+, *i.e.* $\rho_+(t) = \rho(a(t),t)$. For an example of the profile of ρ, see Fig. 4C in the main text.

2.3 General equations

The dynamics of the receptor density, ρ, are described by the continuity equation, $\frac{\partial\rho}{\partial t} = -\boldsymbol{\nabla}\cdot\boldsymbol{j}$, where $\boldsymbol{j} = (j_r, j_\theta)$ is the flux. Due to the circular symmetry, $j_\theta = 0$, and so

$$\frac{\partial\rho}{\partial t} = -\frac{1}{r}\frac{\partial}{\partial r}\left(r j_r\right). \tag{S1}$$

The form of the radial flux, j_r, will be specified below. As engulfment proceeds the engulfment, a, increases due to receptors flowing into the $r < a$ region. The rate at which a increases can be found by conservation of receptor number across the $r = a$ boundary. Note that, unlike in (3), the equation for a cannot be derived by considering conservation of the *total* receptor number: since we extend the receptor dynamics to include inwards drift in addition to diffusion, there are always receptors drifting in from $r = \infty$ and so the total receptor number is manifestly not conserved. In some infinitesimal time dt, the number of receptors flowing across $r = a$ is

$N = -j_{r,+} \cdot 2\pi a \cdot dt$, where $j_{r,+}$ is the radial component of the flux evaluated at $r = a$, *i.e.* $j_{r,+}(t) = j_r(a(t), t)$. These receptors bind ligands on the particle, increase the cup edge from a to $a + da$, and result in the local density increasing from ρ_+ to ρ_L. Thus these N receptors can be written as $N = (\rho_L - \rho_+) \cdot 2\pi a \cdot da$. Equating these two expression for N leads to an expression for $\dot{a}$:

$$\frac{da}{dt} = \frac{-j_{r,+}}{\rho_L - \rho_+}. \tag{S2}$$

These two equations, (S1) and (S2), along with the initial conditions $\rho(r, 0) = \rho_0$ and $a(0) = 0$ and relevant spatial boundary conditions, constitute our model of engulfment.

2.4 Pure diffusion model

We consider various models for the radial flux, j_r. First, we recap the passive, pure diffusion mechanism in (3) for which, according to Fick's law, we write $j_r = -D\frac{\partial \rho}{\partial r}$. Then the system we must solve becomes a one-dimensional, one-phase Stefan problem, given by

$$\begin{aligned} \frac{\partial \rho}{\partial t} &= \frac{D}{r}\frac{\partial}{\partial r}\left(r\frac{\partial \rho}{\partial r}\right), \\ \frac{da}{dt} &= \frac{D\rho'_+}{\rho_L - \rho_+}, \end{aligned} \tag{S3}$$

where ρ' is shorthand for $\frac{\partial \rho}{\partial r}$. In fact this is not the conventional Stefan problem, which would instead involve $-\frac{da}{dt}$ rather than $\frac{da}{dt}$ on the left-hand side of the second equation. Instead this is the supercooled Stefan problem, which can be used to describe the freezing of a supercooled liquid. To find a unique solution we need, in addition to the initial conditions and the behaviour of ρ at $r = \infty$, to specify one extra condition.

We find this extra condition by considering the free energy, in particular by requiring that there is no free-energy jump across the boundary $r = a$. As in (3) we consider three contributions to the free energy. Firstly, we consider the binding between receptors and ligands, which reduces the energy. If each receptor-ligand bond decreases the energy by $-\mathcal{E}k_BT$, then the total binding energy, given that binding only occurs in the bound region (where $\rho = \rho_L$), is given by $-\pi a^2 \rho_L \mathcal{E} k_B T$. Secondly, we consider the energy contribution due to bending of the membrane. As suggested in (5), the bending energy per unit area is given by $\frac{1}{2}(2H)^2 \mathcal{B} k_B T$, where $\mathcal{B}k_BT$ is the elastic bending modulus and H is the mean curvature. We have ignored any possible contribution from the Gaussian curvature. For a spherical bead, the mean curvature is

simply given by $1/R$, where R is the radius of the bead. Thus the total bending energy is $2\pi a^2 \mathcal{B} k_B T/R^2$. Finally, we consider the entropy of the receptor distribution. As argued in (6), the entropy per receptor (relative to the initial entropy when $\rho = \rho_0$ everywhere) is $-k \ln \frac{\rho}{\rho_0}$, which means that that free energy due to entropy is $k_B T \int \rho \ln \frac{\rho}{\rho_0} dA$, where the area integral is taken over all space.

We do not explicitly include the membrane tension. However, such a term is likely (at least as a first approximation) to be proportional to the membrane area (see, for example, (7)). Although this neglects the effect of membrane wrinkles (which implies that the initial cup growth does not necessarily increase the tension), it is a plausible first attempt at modelling tension. Since it will then have the same form as the receptor-ligand binding term, such a tension term could be absorbed into a redefinition of $\mathcal{E}$. This suggests that the parameter $\mathcal{E}$ should be interpreted as a combination of both receptor-ligand binding and membrane tension.

With this interpretation, the total free energy can be written as

$$\frac{\mathcal{F}(t)}{2\pi k_B T} = \left(-\tfrac{1}{2}\rho_L \mathcal{E} + \frac{\mathcal{B}}{R^2} + \tfrac{1}{2}\rho_L \ln \frac{\rho_L}{\rho_0} \right) a^2 + \int_a^\infty \rho \ln \frac{\rho}{\rho_0} r dr. \qquad \text{(S4)}$$

By differentiating and using the equation of motion for ρ in Eq. (S3), we find that the rate of change of $\mathcal{F}$ is

$$\frac{\dot{\mathcal{F}}(t)}{2\pi k_B T} = -\rho_L \left(\mathcal{E} - \frac{2\mathcal{B}}{\rho_L R^2} + 1 - \frac{\rho_+}{\rho_L} + \ln \frac{\rho_+}{\rho_L} \right) a\dot{a} - \int_a^\infty \rho D \chi'^2 r dr, \qquad \text{(S5)}$$

where $\chi = \ln \frac{\rho}{\rho_0} + 1$ is the chemical potential per receptor. As in (6), we identify the integral term as the rate of energy dissipation due to receptor diffusion and the first term as the free-energy jump across the $r = a$ boundary. Although it is quite possible that in a real cell free energy is lost across this boundary (via heat dissipation), we assume for simplicity that there is no free-energy jump, which allows us to find the receptor density at the boundary, ρ_+, by solving

$$\frac{\rho_+}{\rho_L} - \ln \frac{\rho_+}{\rho_L} = \mathcal{E} - \frac{2\mathcal{B}}{\rho_L R^2} + 1. \qquad \text{(S6)}$$

Although this must be solved numerically, the most important point is that ρ_+ does not depend on time: as the cup boundary increases, the distribution of receptors changes in exactly the correct way to ensure constant receptor density at the boundary. The fact that ρ_+ is constant is the extra condition that we need to uniquely solve Eqs. (S3).

The solution, as can easily be checked, is given by

$$\rho(r,t) = \begin{cases} \rho_L & \text{for } r < a \\ \rho_0 - AE_1\left(\dfrac{r^2}{4Dt}\right) & \text{for } r \geq a \end{cases}$$
$$a(t) = 2\alpha\sqrt{Dt}, \tag{S7}$$

where $E_1(x) = \int_x^\infty \frac{e^{-u}}{u} du$ is the exponential integral. It is easy to see that ρ_+ is indeed independent of time. The constants α and A cannot be chosen freely, but are given in terms of ρ_+ as follows. Substituting Eqs. (S7) into the second equation in (S3) and eliminating A using Eqs. (S7) evaluated at $r = a$, gives

$$\alpha^2 e^{\alpha^2} E_1(\alpha^2) = \frac{\rho_0 - \rho_+}{\rho_L - \rho_+}, \tag{S8}$$

which determines α. Then once α is known, A is given by $A = (\rho_0 - \rho_+)/E_1(\alpha^2)$.

Unlike the equivalent solution for the conventional Stefan problem, which exists for all ρ_0, this solution only exists when $\rho_0 < \rho_L$. This is a well-known property of the supercooled Stefan problem with a constant initial condition (8). Intuitively, the case $\rho_0 = \rho_L$ corresponds to equal receptor and ligand densities, so that receptors need not be transported to the cup and engulfment is instantaneous. Well-posed problems for $\rho_0 \geq \rho_L$ can be obtained only by some modification of the system such as, for example, by replacing $\rho_+ = \text{const}$ with $\rho_+ \propto \frac{da}{dt}$ as in (8). However, such a boundary condition would not conserve free energy across the cup boundary and so is not considered here.

Since it is unlikely that the real biological initial condition will be exactly $\rho(r,0) = \rho_0$, it is interesting to consider the stability of this solution to perturbations in the initial condition. For the case of the one-dimensional Stefan problem (rather than the circularly symmetric case considered here), it was shown in (9) that $a(t) \sim 2\alpha\sqrt{Dt}$ asymptotically as $t \to \infty$ for all initial conditions $\rho(x,t) = f(x)$ where $f'' < 0$ and $f(\infty) < \frac{1}{4}\rho_L$. Further, in (10), it was conjectured that similar behaviour will persist for all $f(x)$ such that $f(\infty) < \rho_L$. Although this is not identical to the system we consider, it seems likely (and is suggested by numerical simulations) that a similar result holds, so that $a(t) \sim 2\alpha\sqrt{Dt}$ is a fundamental feature of the model.

2.5 Pure drift model

Now we consider a different model where, instead of diffusing, the receptors drift with constant velocity v towards the cup. To implement this, we

consider $j_r = -v\rho$, so that our model, Eqs. (S1) and (S2), becomes

$$\begin{aligned}\frac{\partial \rho}{\partial t} &= \frac{v}{r}\frac{\partial}{\partial r}\left(r\rho\right), \\ \frac{da}{dt} &= \frac{v\rho_+}{\rho_L - \rho_+},\end{aligned} \tag{S9}$$

with the same initial conditions as before ($\rho(r,0) = \rho_0$ and $a(0) = 0$). Again, at infinity, we require that $\rho(\infty, t) = \rho_0$.

Unlike the diffusion model, there is no need to impose an extra boundary condition on $r = a$. By writing $\xi = r\rho$ and changing variables to $\sigma_\pm = r \pm vt$, it can be shown that the unique solution is

$$\begin{aligned}\rho(r,t) &= \begin{cases} \rho_L & \text{for } r < a \\ \rho_0\left(1 + \dfrac{vt}{r}\right) & \text{for } r \geq a \end{cases} \\ a(t) &= \frac{1}{\sqrt{\rho_L/\rho_0} - 1} vt,\end{aligned} \tag{S10}$$

with $\rho_+ = \sqrt{\rho_L \rho_0}$. Since ρ_+ is not a free parameter as in the diffusion case (ρ_+ in the diffusion case can be set by fixing $\mathcal{E}$, $\mathcal{B}$ and R in Eq. (S6)), the free-energy condition, Eq. (S6), will not in general be satisfied and there will be a free-energy jump across the $r = a$ boundary.

2.6 Diffusion and drift model

We can now combine the pure diffusion and pure drift models to consider a model with both diffusion and drift. This requires choosing $j_r = -D\frac{\partial \rho}{\partial r} - v\rho$, so that our model is described by

$$\begin{aligned}\frac{\partial \rho}{\partial t} &= \frac{D}{r}\frac{\partial}{\partial r}\left(r\frac{\partial \rho}{\partial r}\right) + \frac{v}{r}\frac{\partial}{\partial r}\left(r\rho\right), \\ \frac{da}{dt} &= \frac{D\rho'_+ + v\rho_+}{\rho_L - \rho_+},\end{aligned} \tag{S11}$$

again with $\rho(r,0) = \rho_0$ and $a(0) = 0$ as initial conditions and $\rho(\infty, t) = \rho_0$ at spatial infinity. As with the pure diffusion model, we search for an extra condition by considering the free energy. Although the free-energy expression, Eq. (S4), is unchanged, the rate of change of the free energy, Eq. (S5), now has extra contributions, which arise after differentiating the

integral in Eq. (S4). We now find that

$$\frac{\dot{\mathcal{F}}(t)}{2\pi k_B T} = -\rho_L \left(\mathcal{E} - \frac{2\mathcal{B}}{\rho_L R^2} + 1 - \frac{\rho_+}{\rho_L} + \ln \frac{\rho_+}{\rho_L} \right) a\dot{a} \\ - (r j_r \chi)|_\infty - \int_a^\infty \rho (D\chi'^2 + v\chi') r dr. \tag{S12}$$

The term $(r j_r \chi)|_\infty$ represents the free energy flowing in from infinity. This is a consequence of the continuous drift of receptors entering at $r = \infty$ and moving towards the cup boundary. Although infinite, we ignore this term since we are concerned with a potential free-energy jump at $r = a$ rather than at $r = \infty$. The integral now also has a contribution from drift and, as before, we identify this term as dissipation (now due to both diffusion and drift). Thus the potential energy jump across $r = a$ is given by the $a\dot{a}$ term, which is identical to the equivalent term in the pure diffusion case. This means that the condition for not having a free-energy jump across the boundary is unchanged from Eq. (S6), implying that again ρ_+ is a constant, independent of time.

As described below, we find solutions to this system numerically, by using initial conditions taken from the pure diffusion case and imposing constant ρ_+ at each time step.

2.7 Model with signalling

We now extend the model by adding a second species, a signalling molecule, with density S. This signalling molecule is presumed to be produced in the bound region, to diffuse into the unbound region and to interact with the receptors to further encourage cup growth. Although in a real cell signalling molecules may well move throughout the entire cytoplasm, we assume, for simplicity, that our signalling molecules are restricted to the membrane. It is unlikely that relaxing this assumption would lead to any qualitative differences from our simple model. Further, due to the circular symmetry of our model, we can, as with the receptor density ρ, describe the density of signalling molecules only as a function of their radius from the origin. So, as with ρ, we consider $S(r, t)$.

The dynamics of S is controlled by three processes. Firstly, it can diffuse throughout the entire membrane with diffusion constant D_S, which is in general different to D (the receptor diffusion constant). Secondly, S is degraded everywhere, with constant lifetime τ. We consider the simplest possible model, with the rate of degradation proportional to the density of S itself. Finally, we assume that the production of S is stimulated by receptor-ligand bonds and so only occurs in the bound region, *i.e.* where $r < a$.

Within this region we assume that S is produced with a rate that is proportional to the receptor density, ρ_L, with the constant of proportionality given by β. Thus the dynamics of S are described by

$$\frac{\partial S}{\partial t} = \frac{D_S}{r}\frac{\partial}{\partial r}\left(r\frac{\partial S}{\partial r}\right) + \beta\rho_L\Theta(a-r) - \tau^{-1}S, \tag{S13}$$

where $\Theta(x)$ is the Heaviside function, which ensures that S is only produced in the bound region. We assume that initially there are no signalling molecules, so that $S(r,0) = 0$.

To complete the model, we need to couple the behaviour of S to that of ρ. There are various ways this could be achieved, such as producing receptors at a rate proportional to S, or allowing the receptor-ligand binding strength at the cup edge, $\mathcal{E}_+$, to depend on S via, for example, $\mathcal{E}_+ = \mathcal{E}_0 + \mathcal{E}_1 S_+$, where S_+ is the value of S at $r = a$ and $\mathcal{E}_0$ and $\mathcal{E}_1$ are constants. However, we choose to focus on the drift velocity and so allow v to depend on S such that the velocity is higher for larger concentrations of the signalling molecule.

Thus our full model with signalling contains three variables, $\rho(r,t)$, $S(r,t)$, $a(t)$, described by Eqs. (S11) and (S13), with initial conditions $\rho(r,0) = \rho_0$, $S(r,0) = 0$ and $a(0) = 0$. Finally, as previously, we also impose $\rho \to \rho_0$ as $r \to \infty$ for all t and constant receptor density at the cup edge, $\rho(a(t),t) = \rho_+$, where ρ_+ is found by solving Eq. (S6).

2.8 Full model

For the full model, we modify the above setup in two ways. First, we introduce a latent period of time t_0 that represents the initial period when the particle sits on the surface of the cell without any engulfment. During this period there is no engulfment, but there is a non-zero contact area between the particle and the cell, so that $a = a_0$ for $t < t_0$. After t_0, we start the dynamic part of the model with the initial condition $a(t_0) = a_0$.

Second, we use a threshold S_0 to encode the effect of the signalling molecule on the drift velocity. This models the fact that the effect of S on v is likely to be co-operative. Although we could describe this by a Hill function, $v = v_1\frac{S^n}{S_0^n+S^n}$, for some large power n, we choose, for simplicity, to just use the threshold S_0 (which is equivalent to sending $n \to \infty$). Whilst S_+ is less than S_0, there is no drift, with receptor motion only arising from diffusion. However, when $S_+ \geq S_0$, drift is turned on, with constant value v_1 for all $r \geq a$.

2.9 Model with spheroidal particles

So far, only spherical particles have been considered. However, it is relatively straightforward to extend our analysis to other particles. Since we are using a one-dimensional model, we are confined to consider particles with rotational symmetry. An example of such a shape is a spheroid, which are ellipsoids where two of the principal axes have the same length. As such, spheroids are described by two parameters: R_1, the length of the two semi-principal axes parallel to the membrane, and R_2, the length of the remaining semi-principal axis perpendicular to the membrane. The surface of such shapes can be described by

$$\begin{aligned} x =& R_1 \sin v \cos u, \\ y =& R_1 \sin v \sin u, \\ z =& -R_2 \cos v, \end{aligned} \tag{S14}$$

where $u \in [0, 2\pi)$ and $v \in [0, \pi)$. In this representation, the z-axis is the axis perpendicular to the membrane, with $v = 0$ (corresponding to $z = -R_2$) the point of the spheroid that first makes contact with the membrane.

The only change to our model is in the expression for the mean curvature, H, which now depends on the position of the cup edge. This means that Eq. (S6) must be replaced by

$$\frac{\rho_+}{\rho_L} - \ln \frac{\rho_+}{\rho_L} = \mathcal{E} - \frac{2\mathcal{B}H^2}{\rho_L} + 1. \tag{S15}$$

Thus, at any given time, when the engulfment arc length is $a(t)$, we must determine the mean curvature at that arc length. We do this by relating both the arc length and the mean curvature to the parameter v. The curvature is a standard expression given by (11)

$$2H = \frac{R_2 \left[R_1^2(1 + \cos^2 v) + R_2^2 \sin^2 v\right]}{R_1 \left(R_1^2 \cos^2 v + R_2^2 \sin^2 v\right)^{3/2}}, \tag{S16}$$

whereas the arc length is given by an incomplete elliptic integral of the second kind,

$$a = \int_0^v \sqrt{R_1^2 \cos^2 w + R_2^2 \sin^2 w}\, dw. \tag{S17}$$

For a given engulfment, $a(t)$, we numerically solve Eq. (S17) to find v and then use Eq. (S16) to determine H. Finally, this allows us to solve Eq. (S15) for the receptor density at the cup edge, ρ_+.

3 Details of numerical simulations

Whereas analytic solutions are available for the pure diffusion and pure drift cases (Eqs. (S7) and (S10)), more complicated models, such as the diffusion-and-drift model and the signalling model, had to be solved numerically. To do this we considered a spatial lattice with the radius r represented discretely by the set $\{0, \Delta r, 2\Delta r, \ldots, N\Delta r\}$, with $L = N\Delta r$ the total length of the membrane. Although the analytic solutions apply to the infinite membrane case ($L = \infty$), it is numerically necessary to consider a finite membrane which, of course, is also more realistic for a real cell. We used $L = 50\mu$m and $\Delta r = 0.01\mu$m although we checked that smaller values of Δr did not noticeably change the results. At any given time t, the receptor density, the signalling molecule density and the cup position were represented by $\rho_i(t)$, $S_i(t)$ and $a(t)$ respectively, where i labels the spatial position such that $r = i\Delta r$.

The initial values of ρ_i and a were found from Eq. (S7) with $t = \Delta t$ (except in the full model where initially we set $a = a_0$). It is not possible to set the initial values to $\rho = \rho_0$ and $a = 0$ since then engulfment would never start and a would always be zero. Although Eq. (S7) only strictly applies for the pure diffusion model, this makes little difference at $t = \Delta t$. In fact, we found that any small fluctuation in $\rho(r, 0)$ away from ρ_0 leads to practically identical output. The initial value of S_i was set to zero for all i.

At each time step ($\Delta t = 2.5 \times 10^{-5}$s) we considered the finite difference versions of Eqs. (S11) and (S13) and hence calculated approximately the values of $\rho_i(t + \Delta t)$, $S_i(t + \Delta t)$ and $a(t + \Delta t)$. As with Δr, we checked that reducing Δt did not lead to better results. It was also necessary to impose spatial boundary conditions at each time step. At $r = L$ we assumed zero-flux of both receptors and signalling molecules so that $\frac{\partial \rho}{\partial r}\big|_{r=L} = \frac{\partial S}{\partial r}\big|_{r=L} = 0$. Similarly, at the origin we imposed $\frac{\partial S}{\partial r}\big|_{r=0} = 0$. The final boundary condition was set by the requirement that $\rho|_{r=a} = \rho_+$, where ρ_+ was found by numerically solving Eq. (S6) or Eq. (S15). Note that in the case where $\mathcal{E}$ depends on S, the value of ρ_+ had to be calculated anew at each time step. Since a is not usually a multiple of Δr, we found the integer j such that $j\Delta r$ is as close as possible to a and set $\rho_j(t + \Delta t) = \rho_+$.

To check that our numerical solutions correctly approximate the real solutions, we compared the analytic and large-L numerical solutions for the two cases with known analytic expressions (pure diffusion and pure drift), finding little difference.

4 Ways of increasing engulfment speed in the pure diffusion model

The first stage of engulfment is well-described by the pure diffusion model, for which $a = A\sqrt{t}$. We favour the model where the second stage is explained by the addition of drift, with diffusive receptor dynamics replaced by diffusion and drift. However, although it does not match our data as well, it is important to point out that a faster second stage could also be achieved by retaining the pure diffusive mechanism and increasing the prefactor A. Eq. (S7) shows that A can be written as $2\alpha\sqrt{D}$ with α given by Eq. (S8) and ρ_+ by Eq. (S6). The nonlinearity of Eqs. (S8) and (S6) means that it is not obvious how changing various parameters affects A and hence affects the speed of engulfment.

Since D does not appear in Eqs. (S8) and (S6), the dependence on the diffusion constant is trivial and $a \propto \sqrt{D}$ as shown in Fig. S3A. With a greater diffusion constant, the rate of flow of receptors across the cup boundary is larger leading to quicker engulfment. The receptor diffusion constant could easily be altered by modifications to the receptor, such as phosphorylation. However, it seems unlikely that D could be increased by a factor of four, as would be required to fit the second stage.

The receptor density at infinity, ρ_0, only appears in Eq. (S8) and so, as ρ_0 increases towards ρ_L, the value of α tends towards ∞ (Fig. S3B). As discussed above, this is a well-known property of this system, which is ill-posed if $\rho_0 \geq \rho_L$. Thus producing more receptors during engulfment would increase the engulfment speed. However, it is likely that our model will break down well before $\rho_0 = \rho_L$, probably due to free energy not being conserved across the cup boundary, so that ρ_+ becomes dependent on time.

Now we consider the receptor-ligand bond strength, $\mathcal{E}$. Increasing $\mathcal{E}$ increases the right-hand side of Eq. (S6), which, since $\rho_+ < \rho_L$, reduces ρ_+. In turn a reduction in ρ_+ increases the right-hand side of Eq. (S8) and so increases the engulfment speed (Fig. S3C). As $\mathcal{E}$ continues to increase, α tends to a limit given by $\alpha^2 e^{\alpha^2} E_1(\alpha^2) = \frac{\rho_0}{\rho_L}$ and corresponding to $\rho_+ = 0$. Conversely, decreasing $\mathcal{E}$ reduces α and eventually leads to zero engulfment speed for non-zero $\mathcal{E}$. This value of $\mathcal{E}$ occurs when $\rho_+ = \rho_0$ and is found by solving

$$\frac{\rho_0}{\rho_L} - \ln\frac{\rho_0}{\rho_L} = \mathcal{E} - \frac{2\mathcal{B}}{\rho_L R^2} + 1. \tag{S18}$$

An increase $\mathcal{E}$ could be achieved by post-translational modifications of the receptor such as, for example, phosphorylation. However, for our parameter values, a sufficient increase in engulfment speed could not be achieved since

α is already close to its maximum value.

The reverse argument applies to the bending modulus, $\mathcal{B}$, where an increase in $\mathcal{B}$, increases ρ_+ and reduces α (Fig. S3D). Further increasing $\mathcal{B}$ eventually leads to zero engulfment corresponding to $\rho_+ = \rho_0$ and Eq. (S18). An increase in $\mathcal{B}$ would require a change in the membrane structure, perhaps by replacing certain components in order to make bending easier.

The remaining two parameters — the ligand density and the particle radius — cannot easily be altered by the cell to change engulfment speed. However, for completeness, we can still examine their effect on α. The target ligand density, ρ_L, appears multiple times in Eqs. (S8) and (S6), with the result that the effect on α is not obvious and indeed need not even be monotonic. As ρ_L decreases, $\frac{\rho_+}{\rho_L}$ increases, which initially leads to an increase in α. The behaviour on further reduction of ρ_L depends on the exact parameter values. If ρ_L decreases to ρ_0 before ρ_+ increases to ρ_0 then α becomes infinite when $\rho_L = \rho_0$ as in Fig. S3E. However, if $\rho_+ = \rho_0$ before $\rho_L = \rho_0$, the prefactor reaches a maximum, turns round and decreases to zero for non-zero ρ_L. This occurs when ρ_L is given by Eq. (S18).

Finally, as shown in Fig. S3F, increasing the particle radius R reduces the particle curvature, leading to smaller ρ_+ and increased engulfment rate. Conversely, decreasing R eventually leads to zero engulfment when R satisfies Eq. (S18). However, this is not the full story. Although the speed of engulfment is higher for larger particles, there is also a larger particle circumference to engulf. Thus the full engulfment time, $T = \frac{\pi^2 R^2}{A^2}$, is also of interest. This is also plotted in Fig. S3F, showing that T is not monotonic: as also found in (3), there is a critical radius with minimum full engulfment time.

Supporting References

1. Gonzalez, R., and R. Woods. 2007. Digital Image Processing. *Prentice Hall* pp. 728–36.

2. Duda, R. O., and P. E. Hart. 1972. Use of the Hough transformation to detect lines and curves in pictures. *Commun. ACM.* 15:11–15.

3. Gao, H., W. Shi, and L. Freund. 2005. Mechanics of receptor-mediated endocytosis. *Proc. Natl. Acad. Sci. USA.* 102:9469–9474.

4. Tollis, S., A. E. Dart, G. Tzircotis, and R. G. Endres. 2010. The zipper mechanism in phagocytosis: energetic requirements and variability in phagocytic cup shape. *BMC. Syst. Biol.* 4:149.

5. Helfrich, W. 1973. Elastic properties of lipid bilayers: theory and possible experiments. *Z. Naturforsch. C.* 28:693.

6. Freund, L. B., and Y. Lin. 2004. The role of binder mobility in spontaneous adhesive contact and implications for cell adhesion. *J. Mech. Phys. Solids.* 52:2455–2472.

7. van Zon, J. S., G. Tzircotis, E. Caron, and M. Howard. 2009. A mechanical bottleneck explains the variation in cup growth during FcγR phagocytosis. *Mol. Syst. Biol.* 5:298.

8. Myers, T. G., S. L. Mitchell, and F. Font. 2012. Energy conservation in the one-phase supercooled Stefan problem. *Int. Commun. Heat Mass.* 39:1522–1525.

9. Chadam, J., and P. Ortoleva. 1983. The stability effect of surface tension on the development of the free boundary in a planar, one-dimensional, Cauchy-Stefan problem. *IMA J. Appl. Math.* 30:57–66.

10. Dewynne, J. N. , S. D. Howison, J. R. Ockendon, and W. Xie. 1989. Asymptotic behavior of solutions to the Stefan problem with a kinetic condition at the free boundary. *J. Austral. Math. Soc. Ser. B.* 31:81–96.

11. Weisstein, E. W. "Ellipsoid" from *MathWorld – A Wolfram Web Resource*. http://mathworld.wolfram.com/Ellipsoid.html.

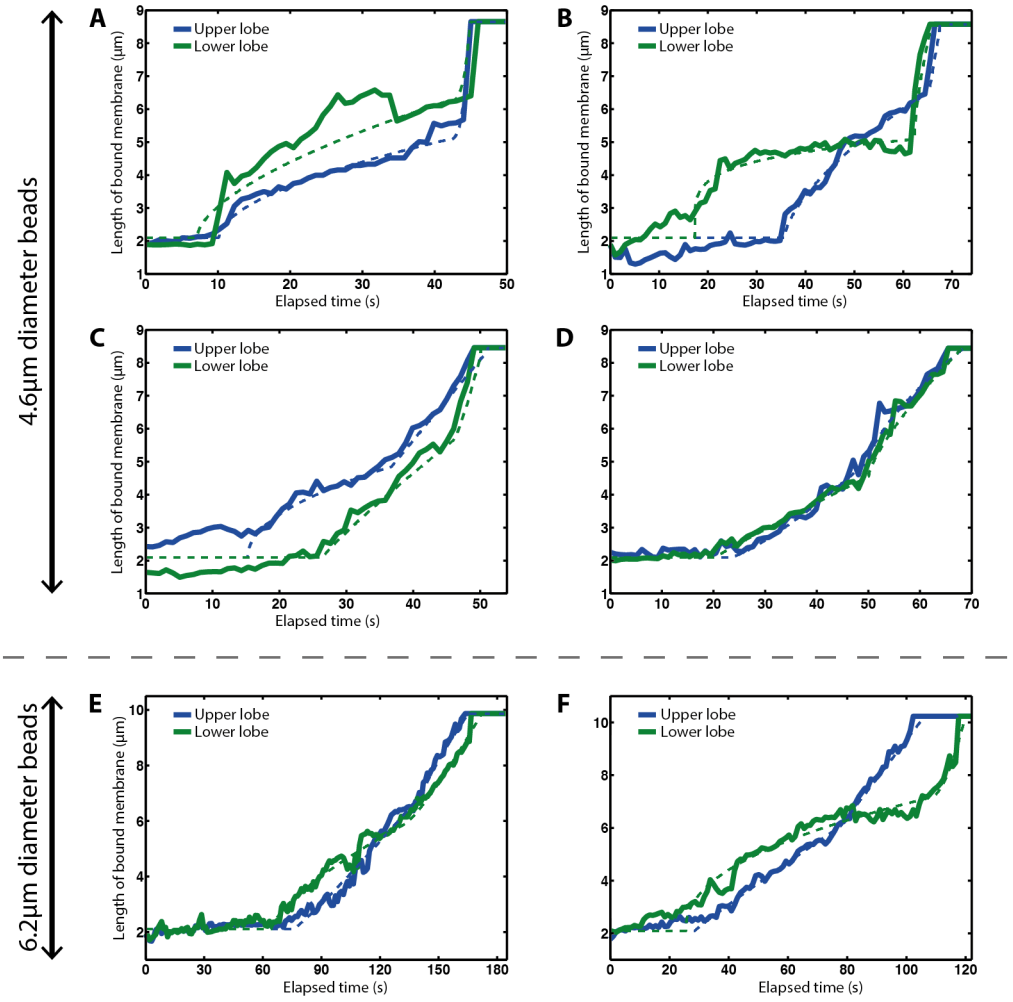

Figure S1: Engulfment against time for all six datasets. Top (blue) and bottom (green) lobes are shown separately. Dashed lines show the best fit to the two-step model (Eq. 1 in main text). (A–D) 4.6μm diameter beads. (E–F) 6.2μm diameter beads.

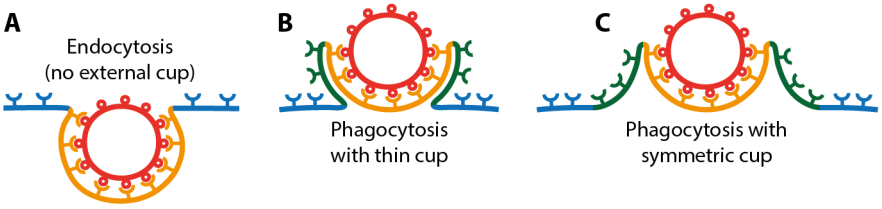

Figure S2: Application of our model to endocytosis and phagocytosis. (A) In endocytosis and CR3-mediated phagocytosis, the particle sinks into the cell leading to membrane bending (the orange region). (B) In Fcγ-mediated phagocytosis the cup leads to extra membrane curvature. In the case of an infinitely thin cup, the curvature of the ligand-bound region of the cup (orange) is exactly equivalent to the curvature of the remaining portion of the cup (green), leading to a four times increase in bending energy (doubling the arc length quadruples the area). (C) The other extreme of a symmetric cup is similar. Although the curvature of the extra curved membrane (green) now has the opposite sign, the contribution to the free energy is the same (the curvature appears squared in the Eq. (S4)). Thus the bending energy is again four times that of the endocytosis model.

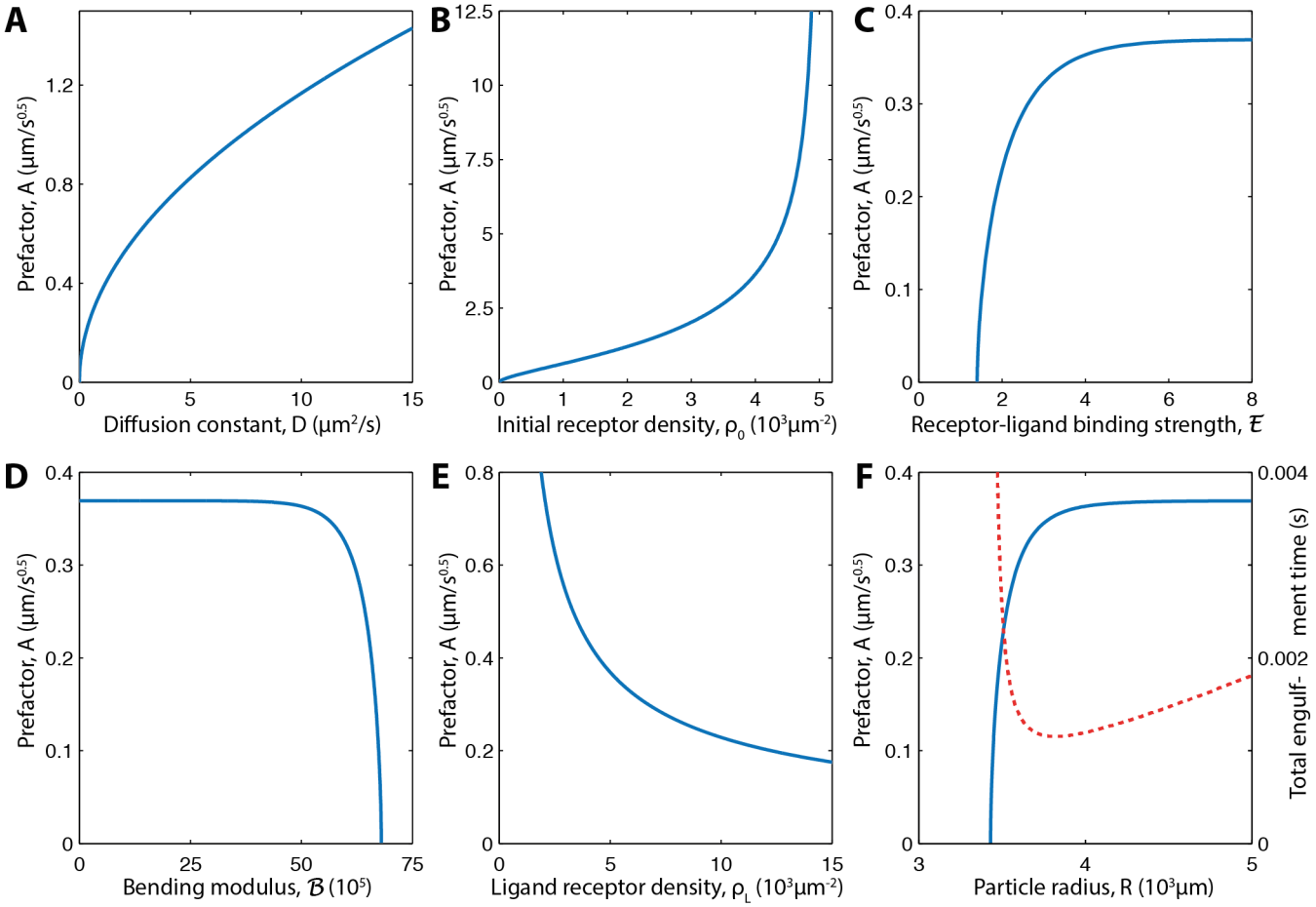

Figure S3: Behaviour of the prefactor $A = 2\alpha\sqrt{D}$ in the pure diffusion model as a function of various parameters. (A) As a function of the diffusion constant, D. (B) As a function of the initial receptor density, ρ_0. (C) As a function of the receptor-ligand binding strength, $\mathcal{E}$. (D) As a function of the bending modulus, $\mathcal{B}$. (E) As a function of the ligand density, ρ_L. (F) As a function of the particle radius, R. In this case, in addition to the prefactor, the total engulfment time is also plotted (dashed red line). In cases (C), (D) and (F), the prefactor drops to zero when Eq. (S18) is satisfied and $\rho_+ = \rho_0$.

Video S1: Example of image analysis. Left: original movie data. Right: automatic image analysis with the cell in blue, the bead in red, the pipette in green and the engulfed region of the membrane in yellow.